

001311



**Modeling the estuarine circulation and fine sediment  
transport associated with subglacial buoyant jets in glacial  
fjords**

by

© Julio Salcedo-Castro

A thesis submitted to the School of Graduate Studies in partial fulfillment of the  
requirements for the degree of

**Doctor of Philosophy**

**Department of Physics and Physical Oceanography**

Memorial University of Newfoundland

**September 2011**

St. John's

Newfoundland

## Abstract

It has been suggested that high latitude systems are one of the regions where the consequences of global warming are becoming more evident. From an oceanographic point of view, glacial fjords are particularly sensitive to climate change because of the seasonal dynamics of sea-ice formation and melting and the important amount of sediment delivered by tidewater glaciers. Our understanding of glacial fjords dynamics in the context of global warming, however, has been the subject of study only during the last two decades. Glacial fjords are estuaries whose complexity arise from a combination of submarine freshwater discharges, as buoyant jets, a highly non-hydrostatic process. Although buoyant jets and sediment transport associated with these processes have received attention through experimental, numerical and field studies, an integrated study of these processes and the estuarine circulation in glacial fjord has been missing. This is explained partly by the difficulty in collecting field data to validate and compare with modeled and experimental results. This thesis describes the estuarine circulation and fine sediment transport associated with a sub-glacial freshwater discharge in a glacial fjord through simplified numerical simulations. Results showed that the discharge of freshwater underneath a glacier into an idealized fjord induces an estuarine-like circulation which is dynamically unstable in the near field, with gradient Richardson number at the sheared interface less than  $< 1/4$ . The dilution factors and velocities of the vertical and surface plumes are strongly and nonlinearly related to the Froude number. The buoyancy flux primarily controls the resulting circulation with the

momentum flux playing a secondary role. Fine sediment transport experiments showed that jet-dominated conditions are more sensitive to the presence of suspended sediment in the discharge than buoyancy-dominated conditions. At high concentrations, sediment settles in the far field, driven by convective sedimentation, and is transported back to the near field by the landward estuarine current. Convective sedimentation is triggered when density is increased by the higher sediment concentration at the interface between the upper and lower layer.

## Acknowledgments

I wish to thank to my supervisor, Daniel Bourgault, for accepting to supervise me as his PhD student and giving me the opportunity to learn more about fjords oceanography and, particularly, glacial fjords. Daniel's advice and guidance helped me to better focus on the essence of the problems and to ignore the unnecessary information.

I am grateful for the comments and guidance provided by Brad deYoung and Sam Bentley. Brad taught me a lot about getting the most out from my results and how to accomplish a good edition of a scientific manuscript. Sam introduced me to the fundamentals of sediment transport and the interesting singularity of fine sediment transport. I also want to thank to Lev Tarasov for his valuable comments and suggestions to improve the thesis manuscript.

This research was carried out through the Circumpolar Flaw Lead (CFL) System Study and funded by the Canadian International Polar Year (IPY) program office and the Natural Sciences and Engineering Research Council (NSERC). Thanks to Memorial University of Newfoundland for awarding me a fellowship from the School of Graduate Studies. I want to thank them for their support which was essential to accomplish this PhD. Especially, I want to thank to the Government of Chile for awarding me the President of the Republic of Chile Fellowship which eased my stay in Canada with my family and allowed me to concentrate on my thesis.

Many thanks to my friends Andry Ratsimandresy and Raúl Cruz who helped me with my poor math skills during the early stage of my PhD.

I want to recognize the love, support and, especially, patience from my family: Lorena, Camila ("Piojita") and Bastián ("Tiancito"). Without their affection and company, my life in Canada would have been very sad and hard.

# Table of Contents

<b>Abstract</b>	<b>ii</b>
<b>Acknowledgments</b>	<b>iv</b>
<b>Table of Contents</b>	<b>viii</b>
<b>List of Tables</b>	<b>ix</b>
<b>List of Figures</b>	<b>xiii</b>
<b>1 Introduction and Overview</b>	<b>1</b>
1.1 Introduction . . . . .	1
1.1.1 Objectives . . . . .	3
1.2 Literature Review . . . . .	4
1.2.1 Glacial fjords . . . . .	4
1.2.2 Sedimentation in glacial fjords . . . . .	7
1.2.2.1 Cohesive sediment and flocculation . . . . .	11
1.2.2.2 Sedimentation from buoyant jets and plumes . . . . .	14
1.2.3 Wall jets and plumes . . . . .	15
1.2.4 Modeling . . . . .	17
1.2.4.1 Modeling of glacial fjords processes . . . . .	17

1.2.4.2	Nonhydrostatic modeling . . . . .	20
1.3	Overview . . . . .	21
1.4	Co-authorship statement . . . . .	22
	<b>Connecting Text</b>	<b>24</b>
<b>2</b>	<b>Circulation induced by subglacial discharge in glacial fjords: Results from idealized numerical simulations</b>	<b>25</b>
2.1	Abstract . . . . .	25
2.2	Introduction . . . . .	26
2.3	Methods . . . . .	29
2.3.1	Model . . . . .	29
2.3.2	Control parameters . . . . .	33
2.4	Results . . . . .	37
2.4.1	Horizontal velocity . . . . .	42
2.4.2	Dilution factor . . . . .	45
2.4.3	Estuarine circulation . . . . .	46
2.5	Discussion . . . . .	53
2.6	Summary and conclusion . . . . .	56
2.7	References . . . . .	57
	<b>Connecting Text</b>	<b>63</b>
<b>3</b>	<b>Modeling ice-proximal fine sediment transport associated with a subglacial buoyant jet in glacial fjords</b>	<b>64</b>
3.1	Abstract . . . . .	64
3.2	Introduction . . . . .	65
3.3	Methods . . . . .	69

3.3.1	Sediment transport . . . . .	69
3.3.2	Flocculation . . . . .	72
3.4	Results . . . . .	76
3.4.1	Plume sediment concentration . . . . .	76
3.4.2	Plume velocity . . . . .	85
3.4.3	Plume dilution . . . . .	86
3.5	Discussion . . . . .	88
3.6	Conclusion . . . . .	91
3.7	References . . . . .	91
<b>4</b>	<b>Summary and conclusions</b>	<b>101</b>
4.1	Conclusions . . . . .	101
4.2	Future work . . . . .	103
<b>5</b>	<b>Bibliography</b>	<b>105</b>

## List of Tables

2.1	Control parameters and non-dimensional numbers for experiments of sub-glacial freshwater discharges. . . . .	36
3.1	Parameters used for sediment transport in the model . . . . .	71
3.2	Typical values of sediment concentration and grain size found in glacial fjords	73
3.3	Parameters used for flocculation in the model . . . . .	74

## List of Figures

2.1	Left: Proposed scheme of the dependence of subglacial jet circulation on the densimetric Froude number ( $Fr$ ) (modified from Syvitski, 1989). Right: Different zones defining the structure of a forced plume entering the sea as a plane jet (VBP: Vertical buoyant plume; HBP: Horizontal buoyant plume) (after Powell, 1990). . . . .	28
2.2	Schematic representation of a glacial fjord, showing parameters considered in the numerical experiments. . . . .	33
2.3	Sequence of density anomaly representing the rising (vertical) plume and spreading of the surface plume observed in a typical momentum-dominated experiment (run # 8, $Fr = 3.16$ ) . . . . .	38
2.4	Sequence of density anomaly representing the rising (vertical) plume and spreading of the surface plume observed in a typical buoyancy-dominated experiment (run # 21, $Fr = 0.1$ ) . . . . .	39
2.5	Sequence representing the evolution of the coefficients of vertical viscosity ( $\nu_e$ ) along the rising (vertical) plume and surface horizontal plume observed in a typical momentum-dominated experiment (run # 8, $Fr = 3.16$ ) . . . . .	40
2.6	Sequence representing the evolution of the coefficients of vertical diffusivity ( $\kappa_e$ ) along the rising (vertical) plume and surface horizontal plume observed in a typical momentum-dominated experiment (run # 8, $Fr = 3.16$ ) . . . . .	41

2.7	(a) Structure of density ( $1 \text{ kg m}^{-3}$ between contour lines) and velocity (largest arrows representing $1.8 \text{ m/s}$ ) and (b) horizontal velocity profile showing a typical estuarine circulation developed in a run buoyancy-dominated (run # 21, $Fr = 0.1$ ). For clarity, only the first 10 meters are shown but the simulated fjord is 100 m deep. . . . .	42
2.8	(a) Horizontal variation of plume velocity as function of distance from the glacier. (b) Horizontal variation of plume dilution as function of distance from the glacier. Velocity, dilution and horizontal distance were nondimensionalized with $u_{max}$ , $S_{max}$ and $H$ , respectively. . . . .	43
2.9	(a) Rate of velocity increase (linear fit) as function of distance along the increasing (transitional) stretch plotted as function of $Fr$ . (b) Same plot corresponding to the decreasing stretch (Note negative sign added to make possible the log fit). . . . .	45
2.10	(a) Rate of dilution increase as function of distance along the fast increasing (transitional) stretch plotted as function of $Fr$ . (b) Same plot corresponding to the slow increasing stretch. . . . .	46
2.11	Variation of plume velocity (a) and plume dilution (b) as a function of $Fr$ at a distance equivalent to $10 d$ , where $d$ is the opening diameter. . . . .	47
2.12	(a) Profiles of gradient $Ri$ number in the top 10 m of the water column (dashed line shows $Ri = 0.25$ ) and (b) plot of minimum $Ri_{min}$ at the sheared interface as function of $Fr$ number at a distance equivalent to $10 d$ , where $d$ is the opening diameter. . . . .	48
2.13	Sequence of density anomaly representing rising (vertical) plume and spreading of surface plume observed in a typical momentum-dominated experiment (run # 8, $Fr = 3.16$ ) . . . . .	49

2.14	Sequence of density anomaly representing rising (vertical) plume and spreading of surface plume observed in a typical buoyancy-dominated experiment (run # 21, $Fr = 0.1$ ) . . . . .	50
2.15	Relationship between the buoyancy flux $B_0$ and the intensity of estuarine circulation, computed as $K_r$ , at a distance equivalent to $10 d$ , where $d$ is the opening diameter. . . . .	51
2.16	Relationship between the buoyancy flux $B_0$ and the potential energy anomaly $\phi$ , at a distance equivalent to $10 d$ , where $d$ is the opening diameter. . . . .	52
2.17	Variation of $K_r/(KE+APE)$ (a) and the ratio $\phi/(KE+APE)$ (b) as function of $Fr$ at a distance equivalent to $10 d$ , where $d$ is the opening diameter. . . . .	53
2.18	Comparison of schemes representing a subglacial discharge. Left: Syvitski (1989) scheme, proposing dependence on $Fr$ only. Right: This study, proposing dependence on $Fr$ and $H/d$ (VBP: Vertical buoyant plume; HBP: Horizontal buoyant plume). . . . .	55
3.1	Schematic representation of a glacial fjord, showing parameters considered in numerical experiments. . . . .	70
3.2	Settling velocity as function of sediment concentration. . . . .	75
3.3	Effect of sediment concentration on $Fr$ number. . . . .	75
3.4	Typical sequence of sediment concentration in a momentum-dominated jet issuing into the ambient denser water (run08, initial jet sediment concentration: $0.1 \text{ kg m}^{-3}$ ). . . . .	77
3.5	Sequence of sediment concentration in the gravity plume spreading at the surface and settling of sediment in the far field (run10, initial jet sediment concentration: $10 \text{ kg m}^{-3}$ ). . . . .	79

3.6	Sequence of sediment concentration in the gravity plume spreading at the surface and settling of sediment in the near field (run10, initial jet sediment concentration: $10 \text{ kg m}^{-3}$ ). . . . .	80
3.7	Sediment concentration profiles (red) taken at a distance equivalent to $10 d$ , where $d$ is the opening diameter (Initial jet sediment concentration: $10 \text{ kg m}^{-3}$ ). Experiments without flocculation are included (black lines) for comparison. . . . .	81
3.8	Sequence of density anomaly field and changes associated with settling of sediment in the far field (run10, initial jet sediment concentration: $10 \text{ kg m}^{-3}$ ). 82	82
3.9	Sequence of density anomaly field and changes associated with settling of sediment in the near field (run10, initial jet sediment concentration: $10 \text{ kg m}^{-3}$ ). . . . .	83
3.10	Effect of sediment concentration on the vertical (a) and horizontal (b) plume concentration for different Fr numbers at a distance equivalent to $10 d$ , where $d$ is the opening diameter. . . . .	84
3.11	Vertical sediment flux (nondimensionalized with the initial jet sediment flux) computed at $10 d$ , where $d$ is the opening diameter. . . . .	85
3.12	Effect of sediment concentration on the vertical (a) and horizontal (b) plume velocity for different Fr numbers at a distance equivalent to $10 d$ , where $d$ is the opening diameter. . . . .	86
3.13	Effect of sediment concentration on the vertical (a) and horizontal (b) plume dilution for different Fr numbers at a distance equivalent to $10 d$ , where $d$ is the opening diameter. . . . .	87

# Chapter 1

## Introduction and Overview

### 1.1 Introduction

Effects of global warming are expected to be strongest in polar regions, where sea-ice cover and duration have declined (Comiso, 2002; Sorteberg and Kvingedal, 2006), and glaciers and ice caps are melting and retreating rapidly (Oerlemans, 1993; Solomon et al., 2007; Straneo et al., 2011). This acceleration of glaciers melting and retreating results from complex feedback between ice melting and oceanographic conditions (e.g. in Greenland) (Holland et al., 2008; Rignot et al., 2010; Straneo et al., 2010; Mortensen et al., 2011; Straneo et al., 2011). Some important consequences of this rapid melting and retreat of glaciers are the increase in meltwater outflow (Solomon et al., 2007) and higher sediment input to coastal marine environments (Hallet et al., 1996; Peizhen et al., 2001; Koppes and Hallet, 2002).

Glaciers that terminate in the sea and discharge ice (icebergs) through calving are called tidewater glaciers (Viel, 2011). Most tidewater glaciers are fast-flowing, have intense crevasseing and terminate in nearly vertical ice cliffs up to 80 m high (Warren, 2011). Some authors have defined “tidewater outlet glaciers” (or outlet glaciers) to refer to glaciers that

discharge ice from ice caps or ice sheets into glacial fjords (Vieli, 2011). In tidewater glaciers, freshwater can result from ice melting at the submerged glacier face or from a combination of supraglacial flows and englacial or subglacial freshwater discharges.

Previous oceanographic studies related to glacial fjords were initially focused on the submarine ice melting at the glacier face and icebergs, and the resulting buoyant plume (Neshyba, 1977; Josberger, 1978; Josberger and Martin, 1981; Neshyba and Josberger, 1980; Home, 1985). Subsequent studies tackled the probable structure of the buoyant jet that provides the freshwater inflow in glacial fjords but their structure has been described mainly in qualitative terms and without reference to structure of the water column or estuarine circulation (Syvitski, 1989; Powell, 1990; Russell and Amott, 2003; Mugford and Dowdeswell, 2011). Sediment transport by these discharges has been inferred from temporal and spatial variability of sediment characteristics and distribution in the water column and on the bottom, but it has not been related to the characteristics of the subglacial buoyant jet (Powell, 1990; Domack and Williams, 1990; Cowan and Powell, 1991; Hill et al., 1998; Curran et al., 2004; Trusel et al., 2010; Mugford and Dowdeswell, 2011). The main reason for this lack of information is that subglacial discharges are more frequent and intense during the melting season (Powell, 1990; Cowan, 1992) when calving is more intense (van der Veen, 2002): calving is a problem for mooring instruments, making it difficult to make direct measurements. Therefore, an estimate of the relationship between the characteristics of the subglacial buoyant jet and the estuarine circulation and sediment transport in the adjacent coastal zone would provide valuable information about the processes taking place in glacial fjords.

Since glaciers are melting and retreating more rapidly, it is necessary to have a quantitative estimate of the impact of glaciers melting and sediment load on the adjacent coast. The links between the tidewater dynamics and the characteristics of the glacial marine environment have been well documented. The concentration of total suspended solids and the

extension of sedimentation processes in a glacial fjord influence some characteristics such as heat exchange with atmosphere, flocculation of colloids and aggregation of particles (influence on carbon flux), physical-chemical and geotechnical properties of the sea floor and the extent of the photic zone (Svendsen et al., 2002). Suspended solids also have a direct impact on organisms living both in the water column and in bottom sediments. Thus the high sediment load in glacial fjords has a strong influence on the structure and distribution of planktonic and benthic communities (Görllich et al., 1987; Hop et al., 2002; Fetzer et al., 2002; Etherington et al., 2007). Massive zooplankton mortality caused by osmotic shock has also been observed (Węśławski and Legeżyńska, 1998; Zajączkowski and Legeżyńska, 2001).

This thesis investigates the relationship between the characteristics of subglacial buoyant jets and the estuarine circulation and fine sediment transport in glacial fjords. I took a fundamental perspective, using a simplified setting in order to better understand the main forcing under study, the buoyant jet. This simplification implies using a 2D modeling and discarding other potentially important forcings, like tides and wind; discarding some initial conditions, like stratification and pulse-like discharges; and dispensing with the wall shear stress on the glacial face and heat exchange with surrounding water. As a consequence, this approach imposes some constraints to the conclusions that can be drawn from this study. However, these results lay the foundations for future investigations on subglacial buoyant jets, estuarine circulation and sediment transport in more complex scenarios.

### **1.1.1 Objectives**

My general objective was to study hydrodynamic and hydrographic responses in the ice-proximal zone of glacial fjords to subsurface freshwater and sediment discharges.

My specific objectives were:

1. To determine relationships between quantities that characterize the steady-state estu-

arine dynamic (e.g. surface layer thickness, stability, strength of estuarine circulation) and characteristics of subglacial buoyant jets.

2. To examine characteristics (e.g. velocity, dilution) of the freshwater/sediment plume rising against the face of the glacier in relation to forcing parameters.
3. To test certain conceptual models, such as the Syvitski (1989) Froude number model upon which the buoyant jet characteristics depend.
4. To describe the transport of cohesive sediment brought into the fjord by a subglacial buoyant jet, for different sediment concentrations and jet conditions.

## 1.2 Literature Review

### 1.2.1 Glacial fjords

Fjords are highly stratified estuaries created by glacial carving and often characterized by one or more submarine sills separating deep basins (Syvitski and Murray, 1981). The main characteristics of fjords are their large length  $L$  to width  $W$  ratio (i.e.  $L/W \gg 1$ ), and their steep sides and great depths compared to the adjacent continental shelves (Farmer and Freeland, 1983).

The principal areas where fjords are located are the western coasts of North and South America (above about  $45^\circ$  latitude), the Kerguelen Islands and parts of Kamchatka, the western coasts of mainland Europe and Britain (north of  $56^\circ$  N in Scotland), the coasts of Spitsbergen, Iceland and Greenland, the Canadian Arctic Archipelago, the coasts of Labrador and Newfoundland, the southwest coast of South Island, New Zealand, the open coasts of Antarctica and of South Georgia, and other high latitude islands (Farmer and Freeland, 1983). Gilbert (1983) gives a more specific definition for arctic and subarctic fjords, defining them as those which are influenced by the presence of sea ice through at

least part of the year, including fjords of the Arctic Archipelago from Ellesmere Island to Baffin Island, and of the east coast from northern Labrador to the Gulf of St. Lawrence. Moreover Gilbert (1983) separates arctic and subarctic fjords from mid-latitude fjords based on that arctic fjords receive a lesser amount of runoff and this flow occurs only during brief summer periods; that sea ice influences fjord processes; and calving glaciers and icebergs contribute fresh water and sediment, in some cases, at considerable depth.

Fjords generally receive most of their freshwater from a river source at the head of the fjord (Farmer and Freeland, 1983). This freshwater drives an estuarine circulation, with brackish water moving seaward at the surface and a compensating lower seawater layer flowing landward. However, as glacial fjords are bound at the head by tidewater glaciers, the freshwater input comes from the subsurface meltwater that rises as a buoyant plume ("upwelling"), entrains seawater along the glacier face, and then spreads horizontally as a gravity current at the surface or at mid depth (Curran et al., 2004). This particular kind of fjord, known as a glacial fjord, is not uncommon, Syvitski (1989) estimated that 25% of the world's fjords are under the influence of tidewater glaciers or floating glaciers.

In glacial fjords, freshwater can arise from a combination of supraglacial flows (from melting at the top of glacier), ice melting at the front (submerged and emerged) of the glacier, and subsurface freshwater discharges which can be at middle depth (englacial) or underneath the glacier (subglacial). Concerning to the relative importance of these freshwater sources, Matthews and Quinlan (1975) hypothesized that, during summer, glacial ice melting could be masked by the much larger input coming from subglacial streams. Cowan (1992) also concluded that the influence of glacier melting is minor compared with the discharge of meltwater from the subglacial tunnel.

Glacial meltwater discharges influence the distribution of physical characteristics of glacial fjords. Pickard (1967) observed that glacial fjords had lower temperatures (2 – 3°C lower) and a narrower range of salinity and density than non-glacial fjords. Matthews

and Quinlan (1975) described a warm surface layer spreading over a cold tongue from the glacier and stated that tidal glaciers act as a heat sink and a source of oxygenated water. The circulation pattern in glacial fjords is not always dominated by strong estuarine type surface outflows but it can also show midwater and deepwater tongues near the glacial front (Domack and Williams, 1990).

Subsurface discharges in glacial fjords are markedly variable and seasonal (Mackiewicz et al., 1984). In Columbia Bay, Walters et al. (1988) mentioned that the dominant runoff component is the meltwater flow that peaks in summer (over  $300 \text{ m}^3 \text{ s}^{-1}$  versus  $< 10 \text{ m}^3 \text{ s}^{-1}$  in winter). This seasonality was also mentioned by Mackiewicz et al. (1984) and Cowan (1992), who both explained that most of the freshwater enters these fjords during summer from large streams discharged at the base of the water column. More recently, Svendsen et al. (2002) observed that the main freshwater input to the fjord occurs in the summer season, mainly due to the melting of snow and ice, and that 90% of the freshwater is supplied to the fjord during three summer months. Similarly, Motyka et al. (2003) described a strong upwelling during late summer, observing water rising 0.5 m above the surface of the ambient water level; a thick overflow plume (30-35 m) consisting of a mixture of warm seawater and cold freshwater was also observed. Moreover, diurnal variability in melting discharges has been documented by Reed (1988), who observed maximal glacial discharges in the late afternoon and early evening, after the maximum solar radiation in the middle of the day.

One of the first attempts to provide a comprehensive description of the oceanographic processes in glacier-influenced fjords was made by Syvitski (1989). Syvitski (1989) asserted that subglacial or englacial discharges probably take the form of a jet whose behavior depends on the density difference between the plume ( $\rho_0$ ) and the ambient fluid ( $\rho_\infty$ ), and jet momentum. Also, the curvature of the jet axis depends on the distance  $s$  from the point of discharge (the ice tunnel), measured along the axis of the jet, the distance  $r$  from the axis of the jet, the diameter  $d$  of the ice tunnel, the initial jet velocity  $u_0$  and the Froude number:

$$Fr = \frac{u_0}{(g d (\frac{\rho_s - \rho_0}{\rho_0}))^{1/2}}, \quad (1.1)$$

The curvature will be large if  $|Fr|$  is small. When  $|Fr| \sim 0$ , then the jet will be directed vertically upwards immediately after leaving the tunnel. On the other hand, the influence of the initial momentum will depend on the angle ( $\beta$ ) between the tangent to the central axis of the jet and the horizontal plane (for  $\beta = 0$ , the initial momentum predominates; for  $\beta = 90$ , the buoyancy predominates). Furthermore, when the discharge is subglacial, the jet is a plane jet because it interacts with the sea floor, where it decelerates more rapidly because of the bottom friction, whereas englacial discharges are axisymmetric (Powell, 1990). As the momentum flux is commonly small for most stream discharges, in comparison to the buoyancy flux, the jet quickly transforms to a vertical jet and plume (Cowan and Powell, 1990). Russell and Arnott (2003) also stated that when a flow is exiting along the basin floor, the jet is better modeled as a plane-wall jet. The flow can be supercritical ( $Fr > 1$ ) when just leaving the tunnel but then it can slow down and thicken, converting kinetic energy to potential energy ( $Fr < 1$ ) and forming a hydraulic jump.

The main characteristics of the glacial fjords can be summarized as estuaries bound by a vertical ice wall at the head and where, unlike typical fjords, the freshwater inflow is a discontinuous subglacial buoyant jet at the base of the glacier. This discharge is highly seasonal and influences the physical characteristics and sediment distribution in the fjord. The characteristics of the buoyant jet determine its further influence on the adjacent environment but this interaction has not been studied from an integrated perspective.

### 1.2.2 Sedimentation in glacial fjords

About one-tenth of the world's coasts actually present active glacialmarine environments or environments where sediment is finally deposited after being discharged from glacier ice

(Curran et al., 2004). In these environments, glacial fjords present characteristics such as a steep coastline with little or no sediment accumulation on beaches, sediment discharges mostly from only one source, a negligible bedload movement, and high inorganic sedimentation rates (Syvitski and Murray, 1981; Syvitski et al., 1987; Curran et al., 2004).

Sedimentation in glacial fjords is determined by the combination of sediment inflow at the base of the water column or from englacial discharges; the effect of ice calving on proximal sediment; a stratified water mass; and the presence of the glacial front (Mackiewicz et al., 1984; Elverhøi et al., 1983). Additionally, katabatic winds can enhance upwelling at the glacial front and affect sediment transport away from the glacier, as shown by a comparison of suspended sediment between days with and without winds (Cowan and Powell, 1990). Moreover, there could be secondary sediment distribution by slides, gravity flows, creep, waves and tidal action (Syvitski, 1989; Cowan and Powell, 1990).

The presence of a glacier in direct contact with seawater causes a different sedimentation pattern. Recently, Zajaczkowski (2008) compared two glacial fjords, a glacial-contact fjord, with an englacial runoff; and non glacial-contact fjord, with a tidal flat 0.7 km wide between the glacier and the fjord. Suspended particulate matter (SPM) was transported farther into the fjord at the glacial contact fjord and a removal of 71 % of total SPM was caused by tidal pumping and water mixing. Whereas in the glaciated fjord sediment was transported by a buoyant flow of brackish water, in the non-glacial fjord, sediment was transported and mixed in a flow along the bottom of the tidal flat.

Especially in temperate glacial fjords, meltwater plumes are the primary mechanism whereby fine sediment (i.e. silt and clay) is transported (Curran et al., 2004). In one of the first observations of buoyant plumes in glacial fjords, Hartley and Dunbar (1938) described brown zones where surface currents moved away from ice ( $\sim 0.25 \text{ m s}^{-1}$ ) and the water was very muddy and coffee colored. The upwelling of melt-water can elevate the sea surface by 0.1-1.0 m (Walters et al., 1988). In this zone the concentration of suspended matter

may be 50-60 times higher than in the ambient water surrounding the ice front (Syvitski, 1989). Cowan and Powell (1990) observed suspended sediment concentrations averaging  $0.73 \text{ kg m}^{-3}$  at the surface of an upwelling zone that increased up to  $1.4 \text{ kg m}^{-3}$  during summer. Suspended sediment concentration in the overflow can be  $> 0.1 \text{ kg m}^{-3}$  within 1.5 km away of the glacier.

Subglacial discharges have not only been observed in glacial fjords but also in open-marine tidewater ice fronts. One example is the Austfonna ice cap on Nordaustlandet, Svalbard Archipelago, which has a long ( $\sim 200 \text{ km}$ ) open-marine tidewater ice front. High sediment loads in the Austfonna meltwater discharge indicated a subglacial origin and regions of high surface turbidity were often observed to extend some 15 km perpendicular to the ice front (Pfirman and Solheim, 1989).

Sediment modifies the behavior of buoyant jets and their interaction with the ambient water. The suspended sediment load increases the jet momentum and initial velocity which, along with the increased water viscosity from low temperatures, provides greater capacity for meltwater streams to carry large volumes of debris (Syvitski, 1989). This effect is most notorious for fine-grained sand ( $80$  to  $90 \mu\text{m}$ ) but it is less important for sediment sizes less than  $62 \mu\text{m}$  and greater than  $250 \mu\text{m}$  (Mackiewicz et al., 1984). Due to the significant settling velocity of coarser particles in comparison to a parcel of fluid, the progressive settling of particles will produce a more rapid decaying of the jet velocity than that observed in a jet containing only dissolved matter (Syvitski, 1989).

Concentrations of suspended sediment higher than  $30\text{-}40 \text{ kg m}^{-3}$  are necessary to compensate the density contrast between the water spouting from the ice tunnel and normal seawater. However, normal suspended sediment concentrations in inflow to arctic fjords are several orders of magnitude less than that (Gilbert, 1983). When the sediment concentration is very high, much of the sediment consists mainly of coarse sand and gravel (Syvitski, 1989). During large storms, late in the melt season, however, the suspended

sediment load can be exceptionally high (up to five times normal) (Cowan et al., 1988).

In general, meltwater plume sedimentation rates show an exponential decrease away from the glacier. Suspended fine sand and coarse silt sink as single grains whereas finer silt and clay settle down within flocs (Syvitski, 1989; Curran et al., 2004). Gilbert (1982) stated that most of the sediment sinks from the overflow (and thus potentially deposited) within 15 to 20 km from the fjord head, although sedimentary structures are best preserved near the head of the fjords. In this zone, very fine laminae can be preserved because the high sedimentation rate inhibits the bioturbation and bottom currents are weak or absent (Cowan and Powell, 1990; Jaeger and Nittrouer, 1999).

Jaeger and Nittrouer (1999) affirm that deposition of sediment varied from highly non-steady-state at ice-proximal stations to steady-state at a mid-fjord station, with deposition rates that decreased systematically down fjord from  $0.003 \text{ m d}^{-1}$  to  $0.0002 \text{ m d}^{-1}$ , respectively. In this sense, Elverhøi et al. (1983) observed that sediment concentrations in the plume adjacent to the Kongsvegen can reach  $0.3\text{-}0.5 \text{ kg m}^{-3}$  and are deposited at rates between  $0.5$  and  $1 \text{ m y}^{-1}$ , decreasing to  $1 \times 10^{-3}$  –  $5 \times 10^{-3} \text{ kg m}^{-3}$  in central and outer parts of the fjord, where the rate is  $0.05\text{-}0.1 \text{ m y}^{-1}$ . Thus about 90% of the sediment input from Kongsvegen is deposited relatively adjacent to the ice front (Elverhøi et al., 1983). In a recent investigation, Svendsen et al. (2002) observed that during summer particulate inorganic matter (PIM) is  $\sim 0.34 \text{ kg m}^{-3}$  at the glacier front and decreases to  $< 0.02 \text{ kg m}^{-3}$ , 10 km away. In the same area, Zaborska et al. (2006) classified all sediments of the Kongsfjorden as mud, but the proportion of clay and the organic matter concentration in sediments increases with the distance from the glacier.

As observed by Mackiewicz et al. (1984), overflows or interflows have a cyclic nature because of the diurnal and seasonal fluctuations of the discharges and the cyclic tidal currents. Accordingly, sediments have been observed to accumulate in the form of layers at the base of a stratified water body that has a discontinuous or pulsating supply of sediment,

and each layer corresponds to a separate sediment influx episode.

### 1.2.2.1 Cohesive sediment and flocculation

Sediment particles are classified according to their size, following the Wentworth (or Udden-Wentworth) scale (Wentworth, 1922), subsequently modified by Krumbein and Sloss (1963). In this scale, sediment finer than  $62.5 \mu\text{m}$  is commonly referred as fine sediment or mud and includes silt and clays. Given their small size, these particles have very slow settling velocities (e.g., particles between 2 and  $4 \mu\text{m}$  would settle with a velocity of  $3 \times 10^{-6} \text{ m s}^{-1}$  to  $1.4 \times 10^{-5} \text{ m s}^{-1}$ ). On average, these particles would settle 86 cm in one day (Komar, 1976). The settling of cohesive particles, however, cannot be calculated from the relative density, size and shape of the particle, because other processes, such as Brownian motion, local shear, and differential settling, become significant at this level (Dyer, 1995; Shi and Zhou, 2004). Moreover, these fine particles collide with each other and form aggregations or flocs whose size and settling velocity are several orders of magnitude higher than those of individual particles (Partheniades, 1986).

Syvitski (1989) described three different processes causing particles aggregation: flocculation, aggregation, and pelletization. Flocculation consists in the neutralization of the surface ionic charges on the particles by the water ions and the attraction created through van der Waals interaction (Syvitski, 1989; Dyer, 1995). Aggregation is the agglomeration of particles caused by organic films or secretions from organisms. Pelletization is caused by the ingestion of individual particles by zooplankton and the subsequent excretion in the form of fecal pellets. Since the high load of sediment inhibits a significant presence of planktonic organisms in glacial fjords, it is likely that flocculation must be the more important process linked to particles aggregation in these systems.

Among many factors affecting flocculation, concentration is the most important (Burt, 1986). Therefore, flocculation increases the effective settling velocity which in turn be-

comes a function of particle concentration rather than the grain size (Dyer, 1988). However, it is worth pointing out that the settling velocity of mud flocs can be also affected by other processes, such as turbulence, shear or bottom shear stress, floc strength, fractal structure, sediment composition and residence time of flocs (Shi and Zhou, 2004).

The relation between concentration and floc settling velocity is not constant but presents different regimes according to the range of concentration. At very low concentration, aggregation is negligible and the settling velocity ( $w_s$ ) does not depend on concentration (Mehta, 1986). Within a certain range of concentrations, the relationship between  $w_s$  and concentration  $C$ , is found to be of the form:

$$w_s = kC^n \quad (1.2)$$

When the suspended sediment concentration is higher than  $0.1\text{--}0.3 \text{ kg m}^{-3}$  the free settling changes to flocculation settling because of the increased probabilities of particles collision. Above approximately  $2 \text{ kg m}^{-3}$ , the settling velocity decreases with increasing sediment concentration due to the hindrance between particles (Mehta, 1989).

By making measurements *in situ*, Hill et al. (1998) observed that flocs can grow to diameters of the order of 1 mm and sink at speeds of approximately  $0.5 \times 10^{-3} - 3 \times 10^{-3} \text{ m s}^{-1}$ . Measuring flocs in a range of 0.63 - 5.05 mm of equivalent circular diameter, they were able to fit a regression which allowed to estimate a settling velocity of  $1.5 \times 10^{-3} \text{ m s}^{-1}$  for a 1 mm diameter floc in Glacier Bay, Alaska. More recently, You (2004) found that the settling velocity is independent of sediment concentration if the concentration is  $< 0.3 \text{ kg m}^{-3}$ , whereas there is a nonlinear relationship for concentrations between 0.3 and  $4.3 \text{ kg m}^{-3}$ , and a hindered settling regime for concentrations higher than  $4.3 \text{ kg m}^{-3}$ . An empirical formula was proposed (Eq. 1.3):

$$w_s = w_0 \exp(0.9779C - 0.1080C^2), \quad (1.3)$$

where  $w_s$  and  $w_0$  are settling velocities, in  $\text{mm s}^{-1}$ , and  $C$  is the sediment concentration, in  $\text{g L}^{-1}$ .

So far, simple expressions have been used to represent the effect of concentration on flocculation and settling velocity, as shown above. Moreover, new expressions that include turbulence and shear stress have been proposed, such as the formula proposed by Van Leussen (1994) (Eq. 1.4):

$$w_s = -0.001C^{1.3} \frac{(1 + 0.3G)}{(1 + 0.09G^2)}, \quad (1.4)$$

where  $G = (Ps + Pb)/\nu$ ,  $P_s = K_m[(\partial u/\partial z)^2 + (\partial v/\partial z)^2]$ , and  $P_b = g/\rho_0 K_h (\partial \bar{\rho})/\partial z$  ( $K_m$ =vertical eddy viscosity;  $K_h$ =vertical eddy diffusivity), or that proposed by Manning et al. (2007) (Eq. 1.5):

$$w_s = 0.6 + 0.6\tau - 6.7\tau^2 + 0.00052 \text{ SPM}, \quad (1.5)$$

where  $\tau$  is the turbulent shear stress ( $\text{N m}^{-2}$ ) and SPM is suspended particulate matter concentration ( $\text{mg L}^{-1}$ ).

A similar expression was fit for the Tamar estuary by Dyer et al. (2002):

$$w_s = -0.243 + 0.000567 \text{ SPM} + 0.981 G - 0.0934 G^2, \quad (1.6)$$

where SPM is suspended sediment concentration ( $\text{mg L}^{-1}$ ).  $G$  is the turbulent parameter ( $G = (U_*^3/(\kappa\nu z))^{0.5}$ ) ( $\text{s}^{-1}$ ), where  $U_*$  is the friction velocity,  $\kappa$  is the kinematic viscosity and  $\nu$  is the von Kármán's constant, and  $z$  is the height above the bed.

The process of resuspension/deposition of fine sediments at the bottom is more complicated than for cohesiveless sediments, owing to the cohesiveness of particles smaller than  $100 \mu\text{m}$  (Komar, 1976). However, cohesiveness varies with changes in mineral composition, organic matter content, and sediment bulk properties (Komar, 1976). Therefore,

depending on the characteristics of the fine sediment and degree of consolidation, the shear stress or current velocities necessary to start their motion can be significantly higher than those corresponding to coarser sediments. In a recent review of field and laboratory observations, van Rijn (2007) stated that the initiation of motion of fine sediment beds is in the range of  $0.1 - 0.2 \text{ N m}^{-2}$  and cohesive effects become important for particles finer than  $62 \mu\text{m}$ .

#### 1.2.2.2 Sedimentation from buoyant jets and plumes

Field and laboratory studies about sedimentation from buoyant jets and plumes have been mainly focused on non-cohesive sediments (Carey et al., 1988; Sparks et al., 1991; Bursik, 1995; Ernst et al., 1996; Lane-Serff and Moran, 2005). Recently, Lane-Serff (2011) modeled the deposition of cohesive sediment from buoyant jets and found that the fall-speed decreases as the sediment load decreases. Also this author observed that deposition rate was lower near the origin but was higher further away from the source as more sediment remained in the current for longer distances.

Convective sedimentation is a process that has recently been observed in the sediment transport associated with buoyant plumes (McCool and Parsons, 2004). This convection occurs when the stratification hinders the fall speed of the sediment and, as a result, sediment concentrates along the pycnocline, until the region becomes gravitationally unstable and the inhomogeneities in the density field can eventually turn into convective cells (Hoyal et al., 1999; Parsons and Garcia, 2001; McCool and Parsons, 2004). The first laboratory observations about this process, also called "sediment fingering", were done by Green (1987) who stated that this process can be important especially in conditions of high sediment concentration, small particles and weak stratification. Furthermore, Parsons et al. (2001) observed that the convection occurred even at sediment concentrations as low as  $1 \text{ kg m}^{-3}$ , and described the generation of a bottom turbidity current, or hyperpycnal plume over the

bottom.

In synthesis, glacial fjords present characteristics that make them ideal natural laboratories to study sediment transport. Subglacial discharges can transport sediment in very high concentrations. Most of the sediment (especially, the coarser fractions) sinks near to the glacier, whereas the fine sediment can be transported longer distances. The fine sediment (silt and clay) settling is not particle-like but it is affected by different aggregation processes that cause a more rapid deposition through the water column. The most important aggregation process is flocculation, which is primarily concentration-dependent. When sediment is transported by buoyant plumes, a process called convective sedimentation can take place.

### 1.2.3 Wall jets and plumes

As it has been described above, circulation in a glacial fjord results from a combination of freshwater discharges as subsurface buoyant jets; a buoyant wall plume rising along the glacier face; and a horizontal flow spreading at the surface or mid-depth. Wall jets have been studied experimentally (Sharp and Vyas, 1977) and numerically (Huai et al., 2010). Sharp and Vyas (1977) found that wall jets cling to the bottom before going up under the effect of buoyancy, along a distance which is directly related to the Fr number. Similar results were found numerically by Huai et al. (2010). However, both cases consisted of a point source and not a wall jet issuing from a vertical wall.

Buoyant jets or forced plumes originate from sources of both momentum and buoyancy. According to Fischer et al. (1979), however, all buoyant jets behave as plumes after certain distance along the flow. The distance along the plume axis where the initial momentum flux is significant depends on the Morton's length scale,  $l_m$  (Morton, 1959), defined as the ratio of initial momentum flux ( $M$ ) to initial buoyancy flux ( $B$ ) raised to  $2/3$  (for plane jets). In this way, for  $z < l_m$  the buoyant jet is momentum dominated (jetlike) whereas that if  $z > l_m$  flow is buoyancy dominated (plumelike) (Fischer et al., 1979).

An important feature of buoyant jets in fjords is their confinement within the limit imposed by the height of the free surface. The experimental and analytical studies on the effect of confined depth on buoyant jets were begun by Jirka and Harleman (1973) and subsequently complemented by other investigations (Jirka and Harleman, 1979; Lee and Jirka, 1981; Jirka, 1982). Jirka and Harleman (1973) divided a buoyant jet in confined depth into four zones: the buoyant jet; the surface impingement; the internal hydraulic jump; and the stratified counterflow. One of their most important results, however, was to demonstrate that the structure and dilution at each zone can be defined as function of only three dimensionless parameters: the Froude number  $Fr$ , the relative submergence  $H/d$  (where  $H$  is the total depth) and the vertical angle of discharge ( $\theta$ ). Jirka and Harleman (1973) observed that the near-field zone (formed by the buoyant jet; the surface impingement; and the internal hydraulic jump) is stable only for a limited range of Froude numbers and relative submergence. A stable jet was defined as not showing re-entrainment and recirculation cells and the solution defining the limit between stable and unstable conditions was found to be:

$$\frac{H}{d} = 1.84 Fr^{4/3} (1 + \cos^2 \theta)^2 \quad (1.7)$$

This dependence of the stability and mixing of a buoyant jets on  $Fr$  and  $H/d$  in a confined depth has been observed experimentally and modeled in horizontal buoyant jets (Jirka and Harleman, 1973; Jirka, 1982; Sobey et al., 1988) and vertical buoyant jets (Jirka and Harleman, 1979; Lee and Jirka, 1981; Wright et al., 1991; Kuang and Lee, 2001, 2006).

One of the first comprehensive works about turbulent jets and plumes was done by List (1982) who asserted that an increase in momentum with distance along vertical turbulent plumes is observed as a result of the continuous buoyancy flux at the source. Although many studies have concentrated on dilution caused by mixing along the rising jet, Wright et al. (1991) indicated that dilution can be even greater if an internal hydraulic jump is present. However, Kuang and Lee (2006) stated that this hydraulic jump zone may not be

observed.

Vertical buoyant wall plumes have been studied mostly in the field of flames and heat transport (Grella and Faeth, 1975; Ljuboja and Rodi, 1981; Lai et al., 1986; Lai and Faeth, 1987; Sangras et al., 1998, 1999, 2000). In particular, Ljuboja and Rodi (1981) observed a considerably smaller spreading and dilution for this kind of plume, compared with the case of a free vertical buoyant jet (or plume). This idea has also been highlighted by Sangras et al. (1999) who also pointed out that the presence of the wall limits mixing to one side and inhibits the development of large eddies normally present in free buoyant plumes.

Even though all the processes described above have been studied separately, from the perspective of pure fluid mechanics, an analytical and integrated description of a glacial fjord considering these components has not been undertaken.

## 1.2.4 Modeling

### 1.2.4.1 Modeling of glacial fjords processes

To date, there have been some efforts to model buoyant jets in glacial fjords and ice caps. One of the first attempts to model the buoyant jet in a glacial fjord was by Greisman (1979), who investigated the ice melting on a glacier face. Greisman (1979) proposed that the glacier melting below the water line appeared to be the most probable process driving the upwelling observed at the glacier face. Employing a simple equation of state, basic thermodynamics, and laboratory results, the melt rate per unit area  $m$  of a vertical ice wall in a stratified ocean was proposed to be:

$$m \propto (\Delta T)^{8/5} \left( \frac{\partial \rho}{\partial z} \right)^{-1/5}, \quad (1.8)$$

where  $\Delta T$  is the temperature difference between seawater in contact with the glacier and the far field seawater; and  $\partial \rho / \partial z$  is the far field density stratification. This equation says that

the melt rate is a strong function of the far field water temperature and weakly dependent upon the density gradient.

MacAyeal (1985) used a stream tube model to examine the evolution of subsurface melt-water plumes and showed that the net vertical penetration of the plume was controlled by the ice melting along the plume path in contact with the glacier face, driven by turbulent entrainment of ambient seawater. In a recent investigation, Mugford and Dowdeswell (2011) used an integral jet model that conserved volume, momentum, buoyancy, and sediment flux along the path of a turbulent buoyant plume and included an empirical expression to represent flocculation. The model results were in good agreement with sedimentation observed in McBride Glacier (Alaska).

In a broader context, freshwater runoff into glacial fjords have also received attention during the last decade. Motyka et al. (2003) applied a model for convective flow in proglacial waters and calculated that 88.7% of the total discharge of the plume was entrained seawater. From the other 11.3%, subglacial discharge represented 10.8% and only 0.5% came from ice melting. The significance of the freshwater runoff was also highlighted in a recent study in Glacier Bay by Hill et al. (2009), who estimated that the freshwater runoff could range between a few hundreds to a few thousands  $\text{m}^3 \text{s}^{-1}$  but the discharges could peak up to  $10000 \text{ m}^3 \text{ s}^{-1}$  during extreme events.

Given the importance of sediments in fjords and estuaries, much modeling efforts have been focused on this subject. Some of these efforts have been specifically focused on glacial fjords. Syvitski and Andrews (1994) used a numerical model to evaluate the changes in the fluvial sediment outputs for two contrasting climate-change scenarios (warmer summers versus warmer and moister winters) in the eastern Canadian Arctic and established that the largest impact would be observed during warmer summers, by causing ice caps to melt and induce more expansive and turbid river plumes, increase the progradation of the coastlines, raise the relative sea level, and increase the number and size of turbidity currents generated

off river mouths.

A modeling of sedimentation of suspended particulate from fluvial plumes in the distal region of a fjord was undertaken by Bursik (1995). In this model, it was assumed that the particle suspension was sufficiently dilute that it did not affect plume density. The results suggested that the empirical modeling of the sedimentation from fluvial plumes was also derivable from physical reasoning by including the governing dynamical principles of buoyancy and sedimentation (Bursik, 1995). In a similar approach, Liu (2005) used a vertical two-dimensional model to investigate the influence of settling velocity on cohesive sediment transport under low flow conditions in the Tanshui River estuary. The results of the model were in qualitative agreement with the available data. However, Liu (2005) recognized that although the settling velocity was expected to increase with the size, large flocs could have smaller density and there was not a unique relation between floc size and settling velocity. Thus, flocculation is a complex process whose dependence on chemical and physical parameters make difficult to include it in quantitative and analytical models.

From a perspective of glacier dynamics, Oerlemans (1993) used a total mass budget, including sediment transport, to simulate the advance-retreat cycle of a tidewater glacier and could link the glacier advance and sediment accumulation to the climatic forcing. Similarly, Mugford and Dowdeswell (2007) used a stratigraphic simulation model to compare the sedimentation between a meltwater-dominated glacier and an iceberg-dominated glacier. In both cases a two-dimensional model accounted for the conservation of mass, momentum, buoyancy and sediment flux along the path of the turbulent, entraining plume flowing into a stably stratified ambient fluid. The application of this glacial marine sedimentation model was able to link the environmental and climatic conditions in these contrasting glaciological settings to the geological formation of distinctive glacial marine deposits (Mugford and Dowdeswell, 2007).

### 1.2.4.2 Nonhydrostatic modeling

Presently, the applications of CFD have taken two main approaches to parameterize turbulence and avoid the high memory and processing work of direct numerical simulations (DNS), which are very demanding in terms of processing and memory because a solution of the complete time-dependent Navier-Stokes equations is sought. Reynolds Averaged Navier-Stokes simulations (RANS) are simulations where equations are time-averaged and space-averaged where turbulence is not completely described as function of time. These simulations save a lot of computational time. Large Eddy Simulations (LES) are simulations where only large eddies are directly computed whereas smaller scale eddies are implicitly solved or modeled through a subgrid scale model (SGS model). In this case, some kind of filtering is used to discriminate large and subgrid fluctuations. Comparatively, LES are closer to observed flow patterns but are more memory and processing demanding than RANS.

Most models used in oceanography consider the hydrostatic assumption as justified when horizontal length scales  $L$  of the motion are several orders of magnitude larger than vertical length scales  $H$  (Cushman-Roisin, 1994), i.e. when

$$H \ll L \quad (1.9)$$

By scaling the continuity equation it can be shown that 1.9 is equivalent to

$$W \ll U, \quad (1.10)$$

where  $U$  and  $W$  are, respectively, characteristic horizontal and vertical velocity scales of the flow.

Under conditions 1.9 or 1.10 the vertical momentum equation can be reduced to the hydrostatic equation. However, in spite of the great advantage in simplifying the numer-

ics and being suitable for modeling large-scale ocean circulation, hydrostatic models are not adequate to reproduce many small-scale processes. Marshall et al. (1997) stated that hydrostatic primitive equations (HPE) begin to break down for flows with horizontal scale between 10 and 1 km.

Compared to standard fjords, glacial fjords present a freshwater inflow entering the fjord at depth, either as subglacial or englacial discharges. This causes a narrow rising plume of freshwater of typical horizontal length scale  $L \sim 1$  m, much smaller than the vertical scale of the plume, typically of order of the fjord depth, i.e.  $H \sim 100$  m. The freshwater forcing in glacial fjord is therefore highly nonhydrostatic since  $H/L \gg 1$ . Standard hydrostatic models can therefore not be used to simulate glacial fjords dynamics, unless the rising plume can be somewhat parameterized. However, there is little information for such a parameterization.

In summary, the modeling efforts related to glacial fjords have been focused on the structure of the subglacial buoyant jet, the freshwater balance and the response of the sediment load associated with tidewater glaciers. These approaches are, however, fragmentary and do not provide a description of the subglacial buoyant jet and the resulting estuarine circulation and fine sediment transport as a whole. Furthermore, a nonhydrostatic model has never been used in order to simulate these processes, in spite of its suitability.

### 1.3 Overview

The present thesis expands the knowledge from existing studies about circulation and sediment transport in glacial fjords, by carrying out fundamental numerical experiments of the process, using a fully nonlinear and nonhydrostatic model set in an idealized 2D configuration. For the sake of simplicity, these numerical experiments did not include ambient stratification, ocean currents, or any ice process, as the main objective of this investigation

was to capture a basic understanding about the flow structure and processes associated with a subglacial discharge in glacial fjords.

The first part of this thesis explored the estuarine circulation in a glacial fjord and looked at the relationship between the characteristics of the subglacial buoyant jet and the structure of the water column in the ice-proximal zone, such as stratification, stability, and the strength of the estuarine circulation. These experiments were set to encompass a range of momentum-dominated to buoyancy-dominated conditions respect to the characteristics of the issuing jet. This work has been published by Salcedo-Castro et al. (2011b).

The second part of the thesis covered the transport of fine sediments (mud) that is injected into a glacial fjord by the subglacial buoyant jet. A number of experiments from the first part was selected to investigate the estuarine circulation and transport of sediment associated with sediment-laden buoyant discharges. The size of the sediment chosen for these experiments demanded to include flocculation as an important component transport of fine grained sediment. This work has been submitted by Salcedo-Castro et al. (2011a) for publication.

The last chapter of this thesis summarizes the main results of this research and highlights some conclusions. Some suggestions for future work are presented in the final chapter.

## **1.4 Co-authorship statement**

Authorship for the first research paper presented in Chapter 2 is listed in the following order: Mr. Julio Salcedo-Castro (thesis author), Dr. Daniel Bourgault (thesis supervisor), and Dr. Brad deYoung (collaborator).

Authorship for the second research paper presented in Chapter 3 is listed in the following order: Mr. Julio Salcedo-Castro (thesis author), Dr. Daniel Bourgault (thesis supervisor), Dr. Sam Bentley (collaborator), and Dr. Brad deYoung (collaborator).

Dr. Daniel Bourgault is a Professor with the Institut des sciences de la mer de Rimouski, Université du Québec à Rimouski (IQAR). Brad deYoung is a Professor with the Department of Physics and Physical Oceanography at Memorial University. Dr. Sam Bentley is a Professor with the Department of Geology and Geophysics at Louisiana State University, USA.

Mr. Salcedo-Castro was responsible for the conception and development of the ideas contained in each research paper. Numerical simulation and data analysis were performed by Mr. Salcedo-Castro. Also, Mr. Salcedo-Castro performed all duties associated with preparing each manuscript. Drs. Bourgault, deYoung and Bentley critically reviewed each manuscript and suggested minor revisions.

## Connecting Text

In order to study the relationship between the characteristics of a subglacial buoyant jet and the associated estuarine circulation in a glacial fjord, a series of fundamental experiments was undertaken. The buoyant jets were defined in terms of buoyancy and momentum dominance, using the Grashof and Reynolds numbers, respectively. The balance between momentum and buoyancy was finally represented by the Froude number. Another important nondimensional number included in these experiments was the relative submergence which accounted for the effect of the finite depth on the evolution of the buoyant jet. It is observed that the estuarine circulation is dynamically unstable in the near field and dependent on the jet Froude number. These conclusions and settings are combined in the Chapter 3 to study the transport of fine sediment carried by a subglacial buoyant jet.

This paper is titled "Circulation induced by subglacial discharge in glacial fjords: Results from idealized numerical simulations". It has been published in *Continental Shelf Research* (Salcedo-Castro et al., 2011).

## **Chapter 2**

# **Circulation induced by subglacial discharge in glacial fjords: Results from idealized numerical simulations**

### **2.1 Abstract**

The flow caused by the discharge of freshwater underneath a glacier into an idealized fjord is simulated with a 2D nonhydrostatic model. As the freshwater leaves horizontally the subglacial opening into a fjord of uniformly denser water it spreads along the bottom as a jet, until buoyancy forces it to rise. During the initial rising phase, the plume meanders into complex flow patterns while mixing with the surrounding fluid until it reaches the surface and then spreads horizontally as a surface seaward flowing plume of brackish water. The process induces an estuarine-like circulation. Once steady state is reached, the flow consists of an almost undiluted buoyant plume rising straight along the face of the glacier that turns into a horizontal surface layer thickening as it flows seaward. Over the range of parameters examined, the estuarine circulation is dynamically unstable with gradient

Richardson number at the sheared interface having values of  $< 1/4$ . The surface velocity and dilution factors are strongly and nonlinearly related to the Froude number. It is the buoyancy flux that primarily controls the resulting circulation with the momentum flux playing a secondary role.

## 2.2 Introduction

Polar regions are particularly sensitive to global climate change since glaciers and ice caps are among the systems that show the most significant response to warming (Solomon et al., 2007). For example, substantial reductions of the sea-ice pack extent may lead to important changes to the structure and function of the Arctic marine environment, such as increases in meltwater outflow (Solomon et al., 2007) and greater sediment input to coastal marine environments (Peizhen et al., 2001).

The connection between ice and ocean boundaries in Arctic environments can be through glacial fjords. In these systems, freshwater can come from supraglacial flows (from melting at the top of glacier), subsurface freshwater discharges which can be at middle depth (englacial) or underneath the glacier (subglacial), or ice melting at the front (submerged and emerged) of the glacier produced by the ambient water. The last process has been proposed as the main mechanism driving the vertical circulation and melt driven upwelling along the glaciers and icebergs face, from a combination of laboratory and theoretical studies (Josberger and Martin, 1981), field observations in the Weddell Sea (Neshyba, 1977), icebergs off NE coast of Newfoundland (Josberger and Neshyba, 1980) and South Cape Fjord (Horne, 1985), and a combination of laboratory and field studies in the Labrador Sea (Josberger, 1978) and the Antarctic (Neshyba and Josberger, 1980).

In some subpolar glacial fjords, however, the glacial ice melting can be masked by the much larger freshwater input from subglacial streams, during the melting season, as

observed in Muir Inlet by Matthews and Quinlan (1975) and in Columbia Bay by Walters et al. (1988). The same conclusion was reached by Mackiewicz et al. (1984) in a study of Muir Inlet, and by Cowan (1992), in a study of McBride Inlet. This has also been stated by Svendsen et al. (2002), in their study of the Kongsfjorden-Krossfjorden system, and, more recently, by Motyka et al. (2003), who applied a model for convective flow in proglacial waters (immediately in front of the glacier face) of LeConte Glacier and estimated that 88.7% of the outflow was entrained seawater, 10.8% from subglacial discharge, and only 0.5% from ice melt. Therefore, besides the importance of the feedback between ocean properties and melt rates on the ice face, it is also necessary to focus on how an alteration of the retreat rate of tidewater glaciers and meltwater outflow will affect the adjacent coastal ocean.

One of the first reviews of the oceanographic processes in glacially influenced fjords was done by Syvitski (1989) and later expanded by Powell (1990). They asserted that subglacial discharges take the form of a buoyant jet whose behavior depends mostly on the density difference between the plume ( $\rho_0$ ) and the ambient fluid ( $\rho_a$ ), the diameter  $d$  of the tunnel opening located at the base or at mid depth of the glacier face, and the initial jet velocity  $u_0$ , all these variables being represented in the Froude number:

$$Fr = \frac{u_0}{(g d (\frac{\rho_a - \rho_0}{\rho_0}))^{1/2}}, \quad (2.1)$$

where  $g$  is the gravitational acceleration. According to this conceptual model, the initial horizontal jet is directed upward immediately after leaving the tunnel for situations characterized with  $|Fr| \sim 0$  (Fig. 2.1, left). In addition, the influence of the initial momentum depends on the angle ( $\beta$ ) between the tangent to the central axis of the jet and the horizontal plane (for  $\beta = 0$ , initial momentum predominates; for  $\beta = 90$ , buoyancy predominates). Therefore, circulation in a glacial fjord during the melting season can be summarized as

a subglacial buoyant jet producing a buoyant wall plume rising along the ice face; and a horizontal buoyant flow spreading at the surface or mid-depth (Fig. 2.1, right).

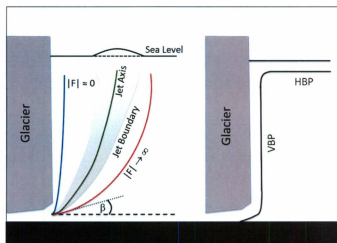


Figure 2.1: Left: Proposed scheme of the dependence of subglacial jet circulation on the densimetric Froude number ( $Fr$ ) (modified from Syvitski, 1989). Right: Different zones defining the structure of a forced plume entering the sea as a plane jet (VBP: Vertical buoyant plume; HBP: Horizontal buoyant plume) (after Powell, 1990).

The effect of confined depth on buoyant jets has been object of many studies. One of the first experimental and theoretical investigations was carried out by Jirka and Harleman (1973) and further studied by others (Jirka, 1982; Jirka and Harleman, 1979; Lee and Jirka, 1981). According to this model, a buoyant jet in confined depth can be schematized into four zones: the buoyant jet; the surface impingement; internal hydraulic jump; and the stratified counterflow. One of the most important results of this model was to establish that the structure and dilution at each zone can be defined as function of only three dimensionless parameters: the Froude number  $Fr$ , the relative submergence  $H/d$  (where  $H$  is the total depth) and the vertical angle of discharge ( $\theta$ ). In this sense, List (1982) has also stated that the vertical motion in turbulent buoyant jets undergoes an increase in momentum with

distance along the path as a result of the continuous buoyancy flux at the source.

Jirka and Harleman (1973) also separated stable and unstable jets in function of these three parameters, where a stable jet was defined as not showing re-entrainment and recirculation cells. This dependence of the stability and mixing of a buoyant jets on  $Fr$  and  $H/d$  in a confined depth has been observed experimentally and modeled in horizontal buoyant jets (Jirka and Harleman, 1973; Jirka, 1982; Sobey et al., 1988) and vertical buoyant jets (Jirka and Harleman, 1979; Lee and Jirka, 1981; Wright et al., 1991; Kuang and Lee, 2001, 2006).

To date, the response of a glacial fjord to a subglacial freshwater discharge has been studied mostly qualitatively based on simplified theories. Here we expand existing studies by attempting to carry out a fundamental numerical study of the process using a fully nonlinear and nonhydrostatic model set in an idealized 2D configuration. These numerical experiments do not include ambient stratification, ocean currents, or any ice processes, as we hope to capture some basic understanding about the flow structure and processes caused only by a subglacial discharge in glacial fjords.

## 2.3 Methods

### 2.3.1 Model

Compared to fjords in general, glacial fjords present freshwater entering the fjord at depth, either as subglacial or englacial discharges. This causes a narrow rising plume of freshwater with a typical horizontal length scale  $L \sim 1$  m, much smaller than the vertical scale of the plume which is roughly the fjord depth, i.e.  $H \sim 100$  m. The freshwater forcing in a glacial fjord is therefore highly nonhydrostatic since  $H/L \gg 1$  (Marshall et al., 1997). Standard hydrostatic models can therefore not be used to simulate glacial fjords dynamics, unless the rising plume could be parameterized in some way. There is, however, no information for

such a parameterization.

In this study, idealized two-dimensional numerical simulations were carried out to understand the plume response to different forcing situations. The model used is a non-hydrostatic, two dimensional, laterally averaged model (Bourgault and Kelley, 2004).

The model has been validated by comparing its results with results from typical problems in fluid dynamics, like lock-exchange flow, shear instability, collision of an internal wave with sloping bottom, and exchange flow through a contracting channel. Moreover, the model was compared with realistic oceanographic conditions, varying the depth and the channel width along the axis of the domain, and with strong nonhydrostatic features (Bourgault and Kelley, 2004).

The chosen model is of the type large eddy simulations (LES), where large eddies are explicitly solved whereas smaller scale eddies are implicitly solved through a subgrid scale model (SGS model). In this case the model uses the Smagorinsky scheme to parameterize subgrid scale turbulence processes. Thus, the mixing length is proportional to the grid size used in the computation i.e. the turbulent viscosity is grid size dependent.

This model uses a finite difference scheme with a variable mesh z-coordinate C-grid and solves the following equations:

$$\frac{\partial u}{\partial t} + u \frac{\partial u}{\partial x} + w \frac{\partial u}{\partial z} = -\frac{1}{\rho_0} \frac{\partial p}{\partial x} + \frac{\partial}{\partial x} \left( v_e \frac{\partial u}{\partial x} \right) + \frac{\partial}{\partial z} \left( v_e \frac{\partial u}{\partial z} \right), \quad (2.2)$$

$$\frac{\partial w}{\partial t} + u \frac{\partial w}{\partial x} + w \frac{\partial w}{\partial z} = -\frac{1}{\rho_0} \frac{\partial p}{\partial z} - \frac{\rho}{\rho_0} g + \frac{\partial}{\partial x} \left( v_e \frac{\partial w}{\partial x} \right) + \frac{\partial}{\partial z} \left( v_e \frac{\partial w}{\partial z} \right), \quad (2.3)$$

along with the two-dimensional continuity equation:

$$\frac{\partial u}{\partial x} + \frac{\partial w}{\partial z} = 0, \quad (2.4)$$

and the advection-diffusion equation for density:

$$\frac{\partial \rho}{\partial t} + u \frac{\partial \rho}{\partial x} + w \frac{\partial \rho}{\partial z} = \frac{\partial}{\partial x} \left( \kappa_e \frac{\partial \rho}{\partial x} \right) + \frac{\partial}{\partial z} \left( \kappa_e \frac{\partial \rho}{\partial z} \right), \quad (2.5)$$

where  $u(x, z, t)$  is the horizontal velocity component;  $w(x, z, t)$  is the vertical velocity (positive upward);  $p(x, z, t)$  is the pressure;  $\rho_0$  is a constant reference density;  $\rho(x, z, t)$  is the density;  $g$  is the gravitational acceleration;  $\nu_e(x, z, t)$ ; and  $\kappa_e(x, z, t)$  are the coefficients of eddy viscosity and diffusivity, respectively. The initial viscosity and diffusivity coefficients were set to  $\nu_e = 1.0 \times 10^{-6} \text{ m}^2 \text{ s}^{-1}$  and  $\kappa_e = 1.0 \times 10^{-7} \text{ m}^2 \text{ s}^{-1}$ , respectively.

Centered differences are used for the spatial derivatives in the momentum and continuity equations as well as diffusion terms in the scalar equation. A second-order limited upstream differencing scheme is used for the advection of scalar quantities in order to reduce the numerical dispersion associated with the centered advection scheme.

Subgrid scale processes of viscosity and diffusivity are parameterized in the model, following Smagorinsky (1963), which is an adaptive scheme depending on the grid spacing and velocity field and uses an adjustable constant of proportionality (Haidvogel and Beckmann, 1999). The Smagorinsky scheme is mostly used in 3D simulations, where important processes like vortex stretching can be better simulated. In 2D simulations, however, important rotational and three dimensional turbulence processes like vortex stretching cannot be modeled. In spite of this fact, the use of the Smagorinsky scheme has proved to be useful in getting valuable information in 2D, stratified 2D (Ozgokmen et al., 2007) and quasi 2D simulations (Awad et al., 2008) which is comparable to the structures observed in 3D modeling (Huang, 2001). Furthermore, the suitability of 2D models to represent turbulence features that are essentially 3D has been previously stated (Batchelor, 1969).

Note that in Bourgault and Kelley (2004) the longitudinal section can have a variable width, represented by a width term  $B$ , whereas equations 2.2-2.5 are written here for a channel of constant width, i.e. for  $B = \text{constant}$ .

The numerical experiments are set in a two-dimensional configuration  $(x, z)$ , a longi-

tudinal section of a glacial fjord, and with freshwater forcing at the glacier face. All the experiments were run with a free surface.

The total length of the numerical domain is 206 km for all simulations with a total depth  $H = 100$  m. The numerical grid has a constant vertical resolution of  $\Delta z = 1$  m. In the horizontal, the grid has a resolution of  $\Delta x = 1$  m for  $0 < x < 100$  m (i.e. the region of interest). For  $x > 100$  m the grid size increases linearly to a maximum of  $\Delta x = 5000$  m. The domain is long compared to the plume width such that the seaward boundary condition does not influence the results. All simulations reached steady state in the region  $x < 100$  m before the freshwater front reached the seaward boundary.

At the bottom, a bottom shear stress is imposed following

$$v \frac{\partial u}{\partial z} \Big|_{z=-H} = -C_D |u_b| u_b, \quad (2.6)$$

where  $u_b$  is the bottom cell horizontal velocity, and  $C_D$  is a drag coefficient given by the law of the wall (Kundu, 1990),

$$C_D = [\kappa / \ln(l/l_0)]^2, \quad (2.7)$$

where  $\kappa = 0.41$  is von Kármán's constant,  $l$  is the height above the bottom, and  $l_0$  is the roughness length, here set to  $l_0 = 1.0 \times 10^{-3}$  m.

At the seaward open boundary, the horizontal velocity  $u$  and density  $\rho$  are calculated using the following radiation condition:

$$\frac{\partial u}{\partial t} + u \frac{\partial u}{\partial x} = 0, \quad (2.8)$$

and

$$\frac{\partial \rho}{\partial t} + u \frac{\partial \rho}{\partial x} = 0, \quad (2.9)$$

respectively. Note however that these seaward boundary conditions have little practical

effect since, as mentioned above, simulations are stopped before the freshwater reaches the seaward boundary.

In all experiments, the glacier was represented as a vertical wall with a no-slip boundary condition. This approach was adopted as part of the simplification in the modeling effort. A further step should be focused on evaluating the effect of friction with the vertical wall representing the glacier. The initial condition was defined as still, uniform density water. The only forcing was a steady flow produced at the open cells set through the glacier face.

### 2.3.2 Control parameters

The control parameters of the simulation are: the total depth of the fjord  $H$ , the opening depth  $h$ , the opening size  $d$ , the jet velocity  $u_0$  and the density difference  $\Delta\rho = \rho_a - \rho_0$ , where  $\rho_a$  is the ambient water density (Fig. 2.2).

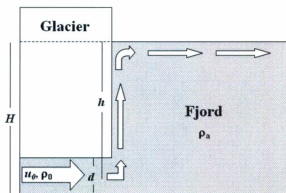


Figure 2.2: Schematic representation of a glacial fjord, showing parameters considered in the numerical experiments.

Two non-dimensional numbers characterize the experiments. The Reynolds number

$$\text{Re} = \frac{u_0 d}{\nu}, \quad (2.10)$$

characterizes the momentum flux; and the Grashof number

$$\text{Gr} = \frac{(\rho_s - \rho_0) g d^3}{\rho_0 \nu^2}, \quad (2.11)$$

characterizes the buoyancy flux, where  $\nu = 1.0 \times 10^{-6} \text{ m}^2 \text{ s}^{-1}$  is the kinematic viscosity of freshwater.

Although some authors have argued that the trajectory of the buoyant jet will depend on these two numbers (Arakeri et al., 2000; He et al., 2002), Angirasa (1999) suggested that the effects of the buoyancy are important only when jet velocities are small. Another number that determines the relative importance of the jet flow and the buoyancy flow, is the Froude number (Eq. 2.1), equivalent to the ratio of inertial to buoyancy forces ( $\text{Fr} = \text{Re}/\text{Gr}^{1/2}$ ) (Arakeri et al., 2000). Therefore there are two limiting cases: when  $\text{Re} \ll \text{Gr}^{1/2}$ , corresponding to a buoyancy-dominated flow; and when  $\text{Re} \gg \text{Gr}^{1/2}$ , which results in a forced convection jet problem.

Another important parameter that characterizes the geometry of the experiment is the relative submergence, defined as the ratio between the total depth and the width of the opening, i.e.:

$$\delta = \frac{H}{d}. \quad (2.12)$$

Although the experiments were defined in terms of the Re-Gr space, the relative submergence and the depth of the opening  $h$  change in different runs as a consequence of varying the opening size  $d$ .

A number of experiments covering a range of buoyancy and jet dominated conditions in a glacial fjord were run. The experiments encompass a range of  $Re$  between  $10^4$  and  $10^6$  whereas  $Gr$  number ranges from  $10^7$  and  $10^{14}$ . The parameter space was set within constraints imposed by the grid size and according to ranges approximately realistic of jet velocity and density differences. The velocity is between  $0.05 - 2 \text{ m s}^{-1}$ , densities ( $\sigma_t$ ) from  $24-28 \text{ kg m}^{-3}$  (corresponding to salinities from 30 to 34). Thus the  $Fr$  varies between 0.02 and 3.8. These experiments are summarized in Table 2.1.

Table 2.1: Control parameters and non-dimensional numbers for experiments of subglacial freshwater discharges.

Run	$d$ (m)	$u_0$ (m s <sup>-1</sup> )	$\Delta\rho$ (kg m <sup>-3</sup> )	Re	Gr	Fr
1	1	0.01	0.001	$1.0 \times 10^4$	$1.0 \times 10^7$	3.2
2	1	0.01	0.010	$1.0 \times 10^4$	$1.0 \times 10^8$	1.0
3	1	0.01	0.102	$1.0 \times 10^4$	$1.0 \times 10^9$	0.32
4	1	0.01	1.019	$1.0 \times 10^4$	$1.0 \times 10^{10}$	0.10
5	1	0.01	10.194	$1.0 \times 10^4$	$1.0 \times 10^{11}$	0.030
8	1	0.1	0.102	$1.0 \times 10^5$	$1.0 \times 10^9$	3.2
9	1	0.1	1.019	$1.0 \times 10^5$	$1.0 \times 10^{10}$	1.0
10	1	0.1	10.194	$1.0 \times 10^5$	$1.0 \times 10^{11}$	0.32
11	2	0.05	12.742	$1.0 \times 10^5$	$1.0 \times 10^{12}$	0.10
12	4	0.025	15.928	$1.0 \times 10^5$	$1.0 \times 10^{13}$	0.030
13	7	0.014	29.719	$1.0 \times 10^5$	$1.0 \times 10^{14}$	0.010
18	1	1.0	10.194	$1.0 \times 10^6$	$1.0 \times 10^{11}$	3.2
19	2	0.5	12.742	$1.0 \times 10^6$	$1.0 \times 10^{12}$	1.0
20	4	0.25	15.928	$1.0 \times 10^6$	$1.0 \times 10^{13}$	0.32
21	8	0.125	19.910	$1.0 \times 10^6$	$1.0 \times 10^{14}$	0.10

## 2.4 Results

After issuing horizontally from the tunnel, the jet turns into a vertical plume rising along the glacier face and, after impinging the surface, the plume spreads horizontally and thickens progressively as it moves seaward. This pattern is similar in momentum-dominated conditions (i.e.  $Re \gg Gr^{1/2}$ , Fig. 2.3) and buoyancy-dominated conditions (i.e.  $Re \ll Gr^{1/2}$ , Fig. 2.4). An interesting feature to note is that the vertical plume width does not increase with height in spite of entrainment; instead, it accelerates and reaches a maximum velocity just below the surface layer (about 10 m depth). This would be consequence of the landward flow of the estuarine circulation that is pushing the buoyant jet and vertical plume against the glacier face. Momentum-dominated conditions took longer to reach steady state and exhibited a bulb-shaped structure where the issuing jet protruded horizontally along the bottom before detaching and rising along the wall (Fig. 2.3).

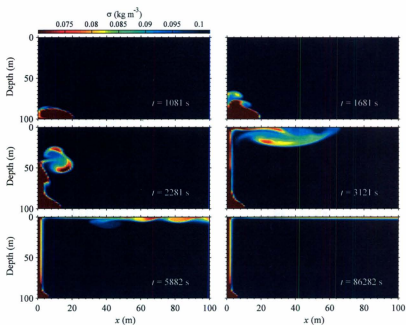


Figure 2.3: Sequence of density anomaly representing the rising (vertical) plume and spreading of the surface plume observed in a typical momentum-dominated experiment (run # 8,  $Fr = 3.16$ )

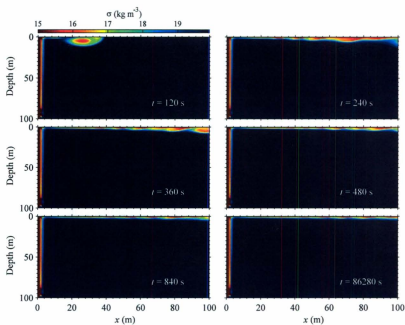


Figure 2.4: Sequence of density anomaly representing the rising (vertical) plume and spreading of the surface plume observed in a typical buoyancy-dominated experiment (run # 21,  $Fr = 0.1$ )

The evolution of the coefficients of vertical viscosity ( $\nu_v$ ) and vertical diffusivity ( $\kappa_v$ ) in run # 8 (momentum-dominated conditions) is shown in Figs. 2.5 and 2.6, respectively. It can be seen that the values of the vertical coefficient of viscosity associated with vertical and horizontal plumes ranged between  $1.0 \times 10^{-6}$  and  $> 1.0 \times 10^{-3} \text{ m}^2 \text{ s}^{-1}$ . On the other hand the values of the vertical coefficient of diffusivity in these regions varied in the same range.

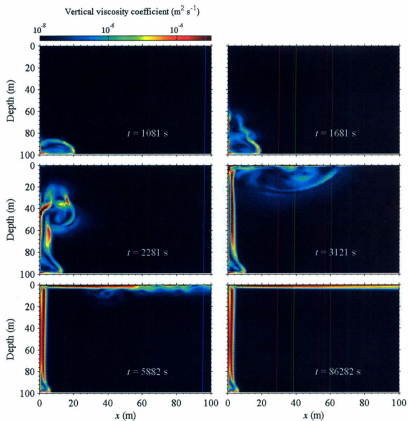


Figure 2.5: Sequence representing the evolution of the coefficients of vertical viscosity ( $\nu_v$ ) along the rising (vertical) plume and surface horizontal plume observed in a typical momentum-dominated experiment (run # 8,  $Fr = 3.16$ )

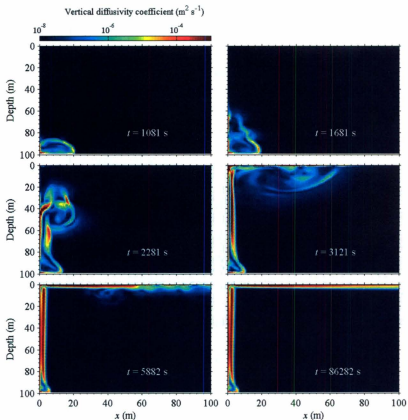


Figure 2.6: Sequence representing the evolution of the coefficients of vertical diffusivity ( $\kappa_v$ ) along the rising (vertical) plume and surface horizontal plume observed in a typical momentum-dominated experiment (run # 8,  $Fr = 3.16$ )

At steady state, the structure observed in all experiments consists of a horizontal wall jet at the bottom, a plume along the glacier face, a surface bulging region and a horizontal surface plume. The surface bulging region is where an uplift of the free surface is produced by the rising vertical plume and a transition to horizontal plume is observed (Fig. 2.7). The

limit between this region and the horizontal surface plume is marked by the point where the upper layer is thinnest. The horizontal circulation is estuarine-like (Fig. 2.7), with a thin ( $\sim 5$  m thick) upper layer moving seaward and a deep lower layer moving toward the glacier (Fig. 2.7).

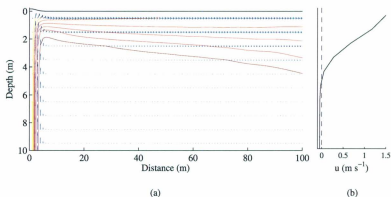
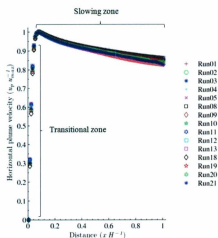


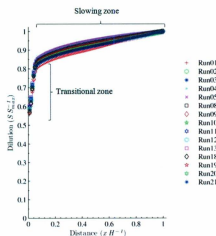
Figure 2.7: (a) Structure of density ( $1 \text{ kg m}^{-3}$  between contour lines) and velocity (largest arrows representing  $1.8 \text{ m/s}$ ) and (b) horizontal velocity profile showing a typical estuarine circulation developed in a run buoyancy-dominated (run # 21,  $\text{Fr} = 0.1$ ). For clarity, only the first 10 meters are shown but the simulated fjord is 100 m deep.

### 2.4.1 Horizontal velocity

The structure of the horizontal velocity at the surface  $u_p$  exhibits two regions (as shown in Fig. 2.8). The first region, immediately following the surface impingement caused by the vertical plume, represents a transitional zone with a sharp linear increase in velocity along the surface. The second region is a decelerating zone, where the plume velocity gradually decreases.



(a)



(b)

Figure 2.8: (a) Horizontal variation of plume velocity as function of distance from the glacier. (b) Horizontal variation of plume dilution as function of distance from the glacier. Velocity, dilution and horizontal distance were nondimensionalized with  $u_{max}$ ,  $S_{max}$  and  $H$ , respectively.

For the transition region, a linear fit was constructed between velocity and distance (non-dimensionalized as  $u_p u_0^{-1}$  and  $x d^{-1}$ , respectively). The slope  $b$  (representing the rate of velocity increase as function of offshore distance in each experiment) was plotted as a function of Fr as shown in Fig. 2.9(a). It can be seen that the velocity increase is higher in buoyancy-dominated experiments (low Fr number) and decreases as the experiments become momentum-dominated (high Fr number).

On the other hand, for the decreasing stretch a logarithmic fit of the form:

$$y = \ln(a x^b), \quad (2.13)$$

was adjusted between non-dimensionalized velocity and distance; where  $b$  represents how quickly  $u_p$  changes as a function of distance from the tunnel ( $b$  positive represents an increase whereas a negative value represents a decrease). The slope  $b$  was plotted as function of Fr and the resultant relationship is shown in Fig. 2.9(b). In this case a negative sign was added to the slope to enable the logarithmic fit. Similar to what was observed in the transitional region, the rate of velocity decrease is higher in buoyancy-dominated experiments and slower for momentum-dominated experiments.

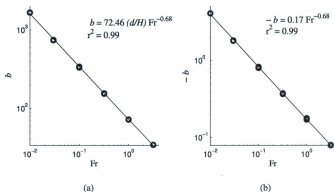


Figure 2.9: (a) Rate of velocity increase (linear fit) as function of distance along the increasing (transitional) stretch plotted as function of Fr. (b) Same plot corresponding to the decreasing stretch (Note negative sign added to make possible the log fit).

## 2.4.2 Dilution factor

In order to evaluate the degree of mixing along the horizontal plume a dilution factor was defined as

$$S = \frac{\rho_a - \rho_0}{\rho_a - \rho_p}, \quad (2.14)$$

where  $\rho_p$  is the plume density, which correspond to the values closest to the surface. These definitions are commonly used in the analysis of plume dilution (Anwar, 1973; Lee and Lee, 1998), and buoyant jets dilution (Chen and Rodi, 1980; Huai et al., 2010). Similar to horizontal velocity, dilution along the surface exhibits two patterns. The first region (transitional zone) shows a linear dilution rate along a short stretch which is followed by a region with a slower dilution rate (Fig. 2.8). A linear fit was applied to the zone nearest to the glacier face. The corresponding slope (representing the rate of dilution increase as function of distance for each experiment) was related to Fr according to the expression shown in Fig. 2.10. On the other hand, a logarithmic fit (Eq. 2.13) was computed for the slow dilution

stretch, and its slope was related to  $Fr$  in a similar way (Fig. 2.10). In this last case it was necessary to add the  $H/d$  ratio to this expression to account for differences in relative submergence between experiments. Buoyancy-dominated experiments (low  $Fr$  number) have a higher dilution rate along the transitional stretch in comparison with momentum-dominated experiments (high  $Fr$  number). A similar pattern is observed when comparing the dilution rate along the slow increasing stretch.

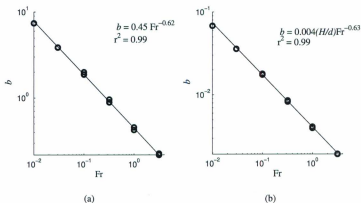


Figure 2.10: (a) Rate of dilution increase as function of distance along the fast increasing (transitional) stretch plotted as function of  $Fr$ . (b) Same plot corresponding to the slow increasing stretch.

### 2.4.3 Estuarine circulation

The response of the estuarine circulation is now assessed by examining the relationship between the surface velocity (normalized by  $u_0$ ) and dilution factor  $S$  and the Froude number at distance  $10d$  from the glacier face. Similarly to the rate of velocity decrease (Fig. 2.9(b)), the velocity of the surface layer is related to  $Fr$  according to a negative power function (Fig. 2.11(a)), implying that the estuarine circulation is mostly driven by the buoyancy flux from the source (subglacial jet issuing at the bottom). As expected, the plume dilution

is also higher at lower Fr (Fig. 2.11(b)), showing a higher entrainment caused by faster velocities at the surface layer.

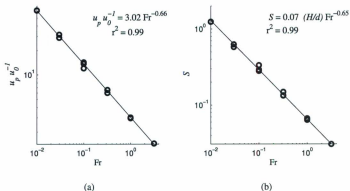


Figure 2.11: Variation of plume velocity (a) and plume dilution (b) as a function of Fr at a distance equivalent to  $10 d$ , where  $d$  is the opening diameter.

The presence of a surface layer with higher velocity and dilution produces a stratified shear flow whose opposite effects of stratification and velocity shear can be characterized in terms of the gradient Richardson number (Thorpe, 1968):

$$Ri = -\frac{g}{\rho} \frac{\partial \rho / \partial z}{(\partial u / \partial z)^2}. \quad (2.15)$$

Similarly to the plume velocity and dilution factor, Ri was computed at  $10 d$  away from the glacier and Ri profiles for the 15 experiments are shown in Fig. 2.12.

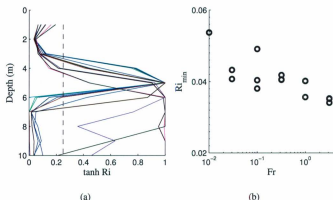


Figure 2.12: (a) Profiles of gradient  $Ri$  number in the top 10 m of the water column (dashed line shows  $Ri = 0.25$ ) and (b) plot of minimum  $Ri_{min}$  at the sheared interface as function of  $Fr$  number at a distance equivalent to  $10d$ , where  $d$  is the opening diameter.

For all experiments the interface was located at 2 m depth, where maximum values of buoyancy frequency and velocity shear occurred (See Eq. 15). The results suggest that  $Ri$  is independent of the characteristics of the buoyant jet, since  $Ri < 1/4$  (average  $Ri = 0.040 \pm 0.005$ ) at the interface in all the experiments (Fig. 2.12). This is confirmed by plotting the minimum  $Ri$  values at the interface as a function of  $Fr$  (Fig. 2.12). Despite favorable conditions for shear instability ( $Ri < 1/4$ ), some experiments (5 of 15 experiments) did not show instabilities at steady-state (Fig. 2.13), presumably because the instabilities are damped by the Smagorinsky scheme for those cases. All other experiments show a continuous growth and decay of shear instabilities at steady state (see for example Fig. 2.4 and Fig. 2.14).

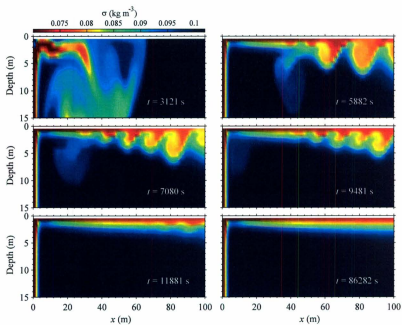


Figure 2.13: Sequence of density anomaly representing rising (vertical) plume and spreading of surface plume observed in a typical momentum-dominated experiment (run # 8,  $Fr = 3.16$ )

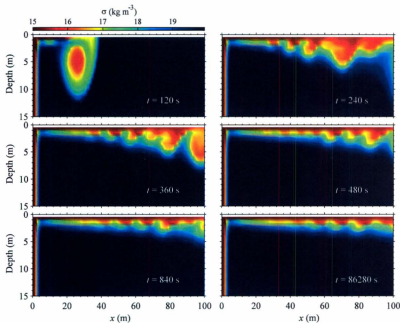


Figure 2.14: Sequence of density anomaly representing rising (vertical) plume and spreading of surface plume observed in a typical buoyancy-dominated experiment (run # 21,  $Fr = 0.1$ )

Another way to assess the fjord response is by comparing the buoyancy flux at the tunnel opening with the intensity of the estuarine circulation. The buoyancy flux ( $B_0$ ,  $m^3 s^{-3}$ ) was computed at the mouth of the tunnel as

$$B_0 = \frac{g d u_0 (\rho_a - \rho_0)}{\rho_a}. \quad (2.16)$$

The intensity of the estuarine circulation was estimated as the vertically integrated kinetic energy density ( $K$ ,  $J m^{-2}$ ), computed at a distance  $10 d$  away from the glacier accord-

ing to

$$K_r = \frac{1}{2} \int_{-H}^{\eta} \rho (u^2 + w^2) dz. \quad (2.17)$$

The estuarine circulation ( $K_r$ ) intensifies as the buoyancy flux ( $B_0$ ) gets higher (Fig. 2.15). This is consistent with results for the surface velocity and dilution since a higher buoyancy flux intensifies the estuarine circulation.

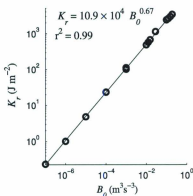


Figure 2.15: Relationship between the buoyancy flux  $B_0$  and the intensity of estuarine circulation, computed as  $K_r$  at a distance equivalent to  $10d$ , where  $d$  is the opening diameter.

The fjord's response can also be assessed by examining how the water column stratification is modified by the freshwater forcing. This is done here by computing the potential energy anomaly (PEA), defined as the equivalent work to homogenize the water column (Simpson et al., 1978; O'Donnell, 2010), ( $\phi$ ,  $\text{J m}^{-2}$ ), which is expressed as

$$\phi = \int_{-H}^{\eta} g (\rho - \bar{\rho}) z dz, \quad (2.18)$$

where  $\bar{\rho}$  represents the depth-averaged density:

$$\bar{\rho} = \frac{1}{H} \int_{-H}^{\eta} \rho(z) dz. \quad (2.19)$$

Similar to  $K_r$ , the PEA was computed at a distance equivalent to  $10 d$  away from the glacier and showed an increase with the buoyancy flux ( $B_0$ ) (Fig. 2.16) .

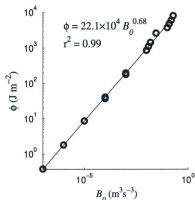


Figure 2.16: Relationship between the buoyancy flux  $B_0$  and the potential energy anomaly  $\phi$ , at a distance equivalent to  $10 d$ , where  $d$  is the opening diameter.

These results of vertically integrated kinetic energy density ( $K_r$ ) and potential energy anomaly ( $\phi$ ), can be related to the total energy input at the source which is represented as the sum of the kinetic energy ( $KE$ ,  $\text{J m}^{-2}$ )

$$KE = \frac{1}{2} u_0^2 d \rho_0, \quad (2.20)$$

and the available potential energy ( $APE$ ,  $\text{J m}^{-2}$ )

$$APE = g d h \Delta \rho. \quad (2.21)$$

It can be seen that the ratio  $K_r/(KE + APE)$  (Fig. 2.17) and the ratio  $\phi/(KE + APE)$  (Fig. 2.17) are similarly related to the Froude number at the source, with an increasing trend as  $Fr$  increases. This result shows that buoyancy-dominated flows exhibit an estuarine

circulation whose energy is very small compared to the total energy influx at the source, and that this proportion increases as  $Fr$  increases.

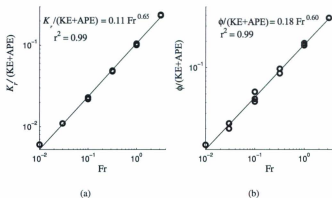


Figure 2.17: Variation of  $K_r/(KE + APE)$  (a) and the ratio  $\phi/(KE + APE)$  (b) as function of  $Fr$  at a distance equivalent to  $10d$ , where  $d$  is the opening diameter.

## 2.5 Discussion

Once steady-state is reached, the structure observed in all the experiments consists of a zone of the wall jet at the bottom, a rising plume along the glacier face and a horizontal surface plume region producing an estuarine circulation. Also, in this last region it was possible to distinguish two zones: a short transition zone with a rapid increase of velocity and dilution, and a larger zone showing a slow decrease of velocity and increase of dilution (Fig. 2.18). These structures have been observed in other numerical and experimental studies of vertical (Jirka and Harleman, 1979; Wright et al., 1991; Kuang and Lee, 2006) and horizontal forced plumes (Jirka and Harleman, 1973; Jirka, 1982). The increase in velocity observed in the transitional zone was caused by the higher pressure gradient caused by the surface elevation when the wall plume reaches the surface. The velocity in the transition zone depends on

the source buoyancy as shown by the relationship between velocity and Fr number in this zone.

The momentum-dominated discharge issuing at the foot of the glacier is a wall jet whose momentum is rapidly lost due to friction with the bottom. In this sense, Powell (1990) mentioned that friction contributes to changing effectively momentum-dominated flows to plume-like flows. This process is not observed in buoyancy-dominated discharges due to a combination of small Fr number and a high submergence ratio that make the flow to rise immediately after leaving the tunnel (Sobey et al., 1988)

From some experimental work on buoyant jets (Jirka and Harleman, 1979; Wright et al., 1991), it is known that Fr can reach values up to 2 orders of magnitude higher than our highest value. Considering this wider range, we can assert that the structures observed in our results correspond to what Syvitski's conceptual model refers as " $Fr \sim 0$ ". However, we propose that Syvitski's conceptual model can be complemented by also considering the relative submergence,  $H/d$ . According to the model proposed by Jirka and Harleman (1973) and Jirka (1982), the structure of buoyant discharges in finite depths is related to Fr and  $H/d$  (also dependent on jet discharge angle). These two parameters are also the base for the criterion of the discharges stability. Therefore, according to this criterion, subglacial buoyant jets can be described as a type of *stable* buoyant discharges, as they are observed to remain attached to the glacier face and do not show recirculation cells up to the surface (Fig. 2.18).

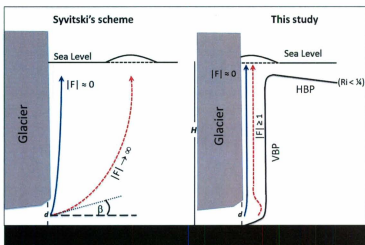


Figure 2.18: Comparison of schemes representing a subglacial discharge. Left: Syvitski (1989) scheme, proposing dependence on  $Fr$  only. Right: This study, proposing dependence on  $Fr$  and  $H/d$  (VBP: Vertical buoyant plume; HBP: Horizontal buoyant plume).

The Richardson number at the sheared estuarine interface is  $< 1/4$  in all the experiments within the first 100 m away from the glacier. The limits and instability of this region are similar to the zone of internal hydraulic jump described in confined buoyant jets by Jirka and Harleman (1973), which exhibits high entrainment rates (Jirka and Harleman, 1979; Wright et al., 1991; Kuang and Lee, 2006) and extends for a horizontal distance equal or greater than  $2.5H$ . This condition suggests that the estuarine circulation is dynamically unstable in the near-field (first 100 m away from the glacier), independently of the forcing conditions, over the parameter space explored here. It is worth mentioning that, in some simulations, the growing of the instabilities could have been prevented by the Smagorinsky subgrid scale model as the eddy diffusivity is increased and instabilities may be inhibited when the shear is stronger than buoyancy, (see Eq. 25 in Bourgalet and Kelley (2004)).

These results show that a small part of the total energy input is converted into estuarine

circulation in buoyancy-dominated cases whereas this conversion is higher in momentum-dominated experiments. In general, stratification and estuarine circulation depend primarily on the buoyancy flux and available potential energy since kinetic energy at the source is relatively smaller and jet momentum is rapidly lost when the jet is issuing from the tunnel. This pattern is characteristic of buoyant jets (Fischer et al., 1979; Powell, 1990).

The nature of the jet at the bottom of the glacier is difficult to observe in nature. In this sense, the quantitative relationships found in this study may be used to obtain an estimate of the characteristics of the subglacial freshwater fluxes from observed far-field density and velocity observations.

Since this investigation considered a simplified scenario, a further step should explore the effect of other variables such as stratification and tides. Another possibility would be simulate pulse-like discharges and include ice wall melting to represent more realistically the behavior of these discharges.

## 2.6 Summary and conclusion

Circulation associated with subglacial freshwater discharge issuing in a glacial fjord is characterized by a combination of a wall jet, a vertical buoyant plume, and a surface plume giving place to an estuarine circulation. There is a transition zone caused by the surface elevation caused by the vertical buoyant plume, where rapid increases of velocity and dilution were observed. The characteristics of the estuarine circulation are related to the Froude number and they are also influenced by the relative submergence  $H/d$ . Buoyancy-dominated discharges showed a more rapid change of velocity and dilution in comparison with momentum-dominated discharges.

The structure of the vertical buoyant plume agrees with the model proposed by Syvitski (1989) since the plume remains attached to the wall (glacier face) for the low Fr magni-

tudes set in the experiments. However, as the circulation is determined by a buoyant jet in confined depth, the relative submergence  $H/d$  is an important parameter to be included. We propose a new schematic diagram for the circulation in glacial fjord, shown in Fig. 2.18.

Buoyancy flux is the most important forcing in subglacial plumes as jet momentum is rapidly lost and processes like mixing, estuarine circulation and stratification are mainly related to the buoyancy flux and the available potential energy.

## 2.7 References

- Angirasa, D., 1999. Interaction of low-velocity plane jets with buoyant convection adjacent to heated vertical surfaces. *Numerical Heat Transfer, Part A* 35, 67–84.
- Anwar, H. O., 1973. Two-dimensional buoyant jet in a current. *Journal of Engineering Mathematics* 7 (4), 297 – 311.
- Arakeri, J., Das, D., Srinivasan, J., 2000. Bifurcation in a buoyant horizontal laminar jet. *Journal of Fluid Mechanics* 412, 61–73.
- Awad, E., Toorman, E., Lacor, C., 2008. Large eddy simulations for quasi-2d turbulence in shallow flows: A comparison between different subgrid scale models. *Journal of Marine Systems* 77, 511–528.
- Batchelor, G. K., 1969. Computation of the energy spectrum in homogeneous two-dimensional turbulence. *Physics of Fluids* 12, 2–233.
- Bourgault, D., Kelley, D. E., 2004. A laterally averaged nonhydrostatic ocean model. *Journal of Atmospheric and Oceanic Technology* 21, 1910–1924.
- Chen, C. J., Rodi, W., 1980. *Vertical turbulent buoyant jets – A review of experimental data*. Pergamon Press.

- Cowan, E. A., 1992. Meltwater and tidal currents: Controls on circulation in a small glacial fjord. *Estuarine, Coastal and Shelf Science* 34, 381–392.
- Fischer, H., List, E. J., Koh, R. C. Y., Imberger, J., Brooks, N. H., 1979. *Mixing in inland and coastal waters*. Academic Press.
- Haidvogel, D. B., Beckmann, A., 1999. *Numerical Ocean Circulation Modeling*. Imperial College Press.
- He, S., Xu, Z., Jackson, J., 2002. An experimental investigation of buoyancy-opposed wall jet flow. *International Journal of Heat and Fluid Flow* 23, 487–496.
- Horne, E. P. W., 1985. Ice-induced vertical circulation in an Arctic fjord. *Journal of Geophysical Research* 90, 1078–1086.
- Huai, W., Li, Z., Qian, Z., Zeng, Y., Han, J., 2010. Numerical simulation of horizontal buoyant wall jet. *Journal of Hydrodynamics* 22, 58–65.
- Huang, M.-J., 2001. Enstrophy cascade and Smagorinsky model of 2d turbulent flows. *The Chinese Journal of Mechanics* 17 (3), 121–129.
- Jirka, G. H., 1982. Turbulent buoyant jets in shallow fluid layers. In: Rodi, W. (Ed.), *Turbulent buoyant jets and plumes*. Pergamon Press, pp. 69–120.
- Jirka, G. H., Harleman, D. R. F., 1973. The mechanics of submerged multiport diffusers for buoyant discharges in shallow waters. Tech. Rep. Technical Report 169, Ralph M. Parsons Laboratory for Water Resources and Hydrodynamics, Massachusetts Institute of Technology, Cambridge, Massachusetts.
- Jirka, G. H., Harleman, D. R. F., 1979. Stability and mixing of a vertical plane buoyant jet in confined depth. *Journal of Fluid Mechanics* 94, 275–304.

- Josberger, E. G., 1978. A laboratory and field study of iceberg deterioration. In: Hussein, A. A. (Ed.), *Iceberg utilization. Proceedings of the first international conference*, Ames, Iowa, 1977. Pergamon Press, pp. 245–264.
- Josberger, E. G., Martin, S., 1981. A laboratory and theoretical study of the boundary layer adjacent to a vertical melting ice wall in salt water. *Journal of Fluid Mechanics* 111, 439–473.
- Josberger, E. G., Neshyba, S., 1980. Iceberg melt-driven convection inferred from field measurements of temperature. *Annals of glaciology* 1, 113–117.
- Kuang, C. P., Lee, J. H. W., 2001. Effect of downstream control on stability and mixing of a vertical plane buoyant jet in confined depth. *Journal of Hydraulic Research* 39, 375–391.
- Kuang, C. P., Lee, J. H. W., 2006. Stability and mixing of a vertical axisymmetric buoyant jet in shallow water. *Environmental Fluid Mechanics* 6, 153–180.
- Kundu, P. K., 1990. *Fluid Mechanics*. Academic Press.
- Lee, J. H. W., Jirka, G. H., 1981. Vertical round buoyant jet in shallow depth. *Journal of the Hydraulics Division, ASCE* 107, 1651–1675.
- Lee, W. T., Lee, J. H. W., 1998. Effect of lateral confinement on initial dilution of vertical round buoyant jet. *Journal of Hydraulic Engineering* 124, 263–279.
- List, E. J., 1982. Turbulent jets and plumes. *Annual Review in Fluid Mechanics* 14, 189–212.
- Mackiewicz, N. E., Powell, R. D., Carlson, P. R., Molnia, B. F., 1984. Interlaminated ice-proximal glacial marine sediments in Muir Inlet, Alaska. *Marine Geology* 57, 113–147.
- Marshall, J., Hill, C., Perelman, L., Adcroft, A., 1997. Hydrostatic, quasi-hydrostatic, and nonhydrostatic ocean modeling. *Journal of Geophysical Research* 102 (C3), 5733–5752.

Matthews, J., Quinlan, A., 1975. Seasonal characteristics of water masses in Muir Inlet, a fjord with tidewater glaciers. *Journal of the Fisheries Research Board of Canada* 32, 1693–1703.

Motyka, R. J., Hunter, L., Echelmeyer, K. A., Connor, C., 2003. Submarine melting at the terminus of a temperate tidewater glacier, LeConte Glacier, Alaska, U.S.A. *Annals of Glaciology* 36, 57–65.

Neshyba, S., 1977. Upwelling by icebergs. *Nature* 267 (5611), 507–508.

Neshyba, S., Josberger, E. G., 1980. On the estimation of Antarctic iceberg melt rate. *Journal of Physical Oceanography* 10, 1681–1685.

O'Donnell, J., 2010. The dynamics of estuary plumes and fronts. In: Valle-Levinson, A. (Ed.), *Contemporary issues in estuarine physics*. Cambridge, pp. 186–246.

Ozgekmen, T. M., Iliescu, T., Fischer, P. F., Srinivasan, A., Duan, J., 2007. Large eddy simulation of stratified mixing in two-dimensional dam-break problem in a rectangular enclosed domain. *Ocean Modelling* 16, 106140.

Peizhen, Z., Molnar, P., Downs, W. R., 2001. Increased sedimentation rates and grain sizes 2 – 3 Myr ago due to the influence of climate change on erosion rates. *Nature* 410, 891–897.

Powell, R. D., 1990. Glacimarine processes at grounding-line fans and their growth to ice-contact deltas. In: Dowdeswell, J. A., Scourse, J. D. (Eds.), *Glacimarine Environments: Processes and Sediments*. Geological Society Special Publication. Vol. 53. The Geological Society, pp. 53–73.

Salcedo-Castro, J., Bourgault, D., deYoung, B., 2011. Circulation induced by subglacial discharge in glacial fjords: Results from idealized numerical simulations. *Continental Shelf Research* 31, 1396–1406.

Simpson, J. H., Allen, C. M., Morris, N. C. G., 1978. Fronts on the continental shelf. *Journal of Geophysical Research* 83, 4607–4614.

Smagorinsky, J., 1963. General circulation experiments with primitive equations. I. The basic experiment. *Monthly Weather Review* 91, 99–164.

Sobey, R. J., J., J. A., Keane, R. D., 1988. Horizontal round buoyant jet in shallow water. *Journal of Hydraulic Engineering* 114 (8), 910–929.

Solomon, S., Qin, D., Manning, M., Chen, Z., Marquis, M., Averyt, K. B., Tignor, M., Miller, H. L. (Eds.), 2007. Contribution of Working Group I to the Fourth Assessment Report of the Intergovernmental Panel on Climate Change, 2007. Cambridge University Press.

Svendsen, H., Beszczynska-Møller, A., Hagen, J. O., Lefauconnier, B., Tverberg, V., Gerland, S., Børre-Orbæk, J., Bischof, K., Papucci, C., Zajaczkowski, M., Azzolini, R., Bruland, O., Wiencke, C., Winther, J. G., Dallmann, W., 2002. The physical environment of Kongsfjorden-Krossfjorden, an Arctic fjord system in Svalbard. *Polar Research* 21, 133–166.

Syvitski, J. P. M., 1989. On the deposition of sediment within glacier-influenced fjords: Oceanographic controls. *Marine Geology* 85, 301–329.

Thorpe, S. A., 1968. A method of producing a shear flow in a stratified fluid. *Journal of Fluid Mechanics* 32, 693–704.

Walters, R. A., Josberger, E. G., Driedger, C. L., 1988. Columbia Bay, Alaska: An 'upside down' estuary. *Estuarine, Coastal and Shelf Science* 26, 607-617.

Wright, S. J., Roberts, P. J. W., Zhongmin, Y., Bradley, N. E., 1991. Surface dilution of round submerged buoyant jets. *Journal of Hydraulic Research* 29, 67-89.

## Connecting Text

This paper studies the transport of fine sediment associated with a subglacial buoyant jet. A set of experiments from Chapter 2 was chosen in order to simulate the transport of cohesive sediment in a glacial fjord. The setting included sediment concentrations ranging from 0.01 - 10 kg m<sup>-3</sup>. Flocculation was also included in the modeling, by using a power law relationship between sediment concentration and sediment settling velocity. The results showed that, at high concentrations, sediment settles in the far field, driven by the convective sedimentation, and is transported back to the ice-proximal zone by the estuarine circulation. The conclusions from this chapter and those from the Chapter 2 are summarized in the Chapter 4.

This paper is titled "Modeling ice-proximal fine sediment transport associated with a subglacial buoyant jet in glacial fjords". It has been submitted to *Marine Geology* (Salcedo-Castro et al., 2011a).

## **Chapter 3**

# **Modeling ice-proximal fine sediment transport associated with a subglacial buoyant jet in glacial fjords**

### **3.1 Abstract**

Fine sediment transport produced by a subglacial freshwater discharge is simulated with a 2D nonhydrostatic model. The circulation pattern revealed a buoyant jet issuing from the tunnel, a vertically buoyant plume and a horizontal surface plume forming part of an estuarine circulation. momentum-dominated experiments are more sensitive to the presence suspended sediment in the discharge. At low concentrations, the sediment stays in the vertical and horizontal plumes and its concentration is progressively decreased by mixing but not noticeable settling is produced through the water column. At high concentrations, the sediment settles in the far field and is transported back to the near field by the landward estuarine current. Sediment came off the surface layer through convective sedimentation, a process that was more effective than flocculation to transport sediment vertically, and

showed vertical velocities faster than  $1.0 \times 10^{-2} \text{ m s}^{-1}$ . Implications of these results are discussed.

## 3.2 Introduction

Approximately one-tenth of the world coastlines are active glacimarine environments or environments where sediment is deposited after being discharged from glacier ice (Curran et al., 2004). Some of these glacimarine environments are glacial fjords (ice fields or glaciers in the hinterland), characterized by high inorganic sedimentation rates, with sediment discharges primarily from a single source (Syvitski and Murray, 1981; Curran et al., 2004).

Changes in sedimentation pattern in glacial fjords can have important consequences on other processes, as sedimentation influence some characteristics such as delivery of nutrients (Apollonio, 1973; Hooze and Hooze, 2002), physical-chemical and geotechnical properties of the seafloor (Sexton et al., 1992), aggregation and vertical flux of particles (influence on carbon flux), heat exchange with the atmosphere, and thickness of the photic zone (Svendsen et al., 2002). Direct impact of suspended solids on the structure and distribution of planktonic and benthic communities has also been well documented (Görlich et al., 1987; Carney et al., 1999; Hop et al., 2002; Fetzer et al., 2002; Etherington et al., 2007).

The estuarine circulation in a glacial fjord during the melting season can be idealized as a subglacial buoyant jet which produces a buoyant wall plume rising along the glacier face, and a gravity current at the surface or mid-depth (Syvitski, 1989; Powell, 1990; Russell and Arnott, 2003; Salcedo-Castro et al., 2011b). The behavior of a buoyant jet depends on the balance between the buoyancy flux, given by the density difference between the plume ( $\rho_0$ ) and the ambient fluid ( $\rho_a$ ); and the momentum flux, represented by the initial jet velocity

$u_0$ . This balance between buoyancy and momentum is represented by the Froude number (Syvitski, 1989; Powell, 1990; Russell and Arnott, 2003; Salcedo-Castro et al., 2011b):

$$Fr = \frac{u_0}{(g d (\frac{\rho_s - \rho_0}{\rho}))^{1/2}}, \quad (3.1)$$

where  $d$  is the opening size and  $g$  is the gravitational acceleration. Thus subglacial discharges can be buoyancy-dominated ( $Fr \sim 0$ ) or momentum-dominated ( $Fr \geq 1$ ) (Syvitski, 1989; Powell, 1990; Salcedo-Castro et al., 2011b).

The character of the sedimentation in glacial fjords is determined by the estuarine circulation caused by the subglacial sediment-laden discharge, the presence of a stratified water mass, and the glacial front (Mackiewicz et al., 1984; Elverhøi et al., 1983). Gilbert (1982) showed that most of the sediment sinks from the gravity current (and is therefore deposited) within 15 to 20 km from the fjord head. Elverhøi et al. (1983) observed that about 90% of the sediment input from Kongsvegen is deposited relatively adjacent to the ice front. Svendsen et al. (2002) found that during summer particulate inorganic matter (PIM) was  $\sim 0.34 \text{ kg m}^{-3}$  at the glacier front and decreased to  $< 0.02 \text{ kg m}^{-3}$ , 10 km away.

Syvitski (1989) has pointed out that the presence of a suspended sediment load increases the initial momentum and velocity of a buoyant jet but a significant settling velocity of particles will produce a more rapid decaying of the jet velocity than that observed in a jet containing only dissolved matter. Thus it is expected that the suspended sediment will affect the buoyant discharges differently, depending on whether they are buoyancy or jet dominated. Studies of sedimentation in glacial fjords have however been primarily focused on bulk sediment and so little is known about fine, cohesive, sediment transport in spite of its predominance in these systems (Syvitski, 1989; Curran et al., 2004). For instance, Zaborska et al. (2006) classified all sediments of the Kongsfjorden as mud, but the proportion of clay and the organic matter concentration in sediments increases with distance from the glacier. A similar conclusion was drawn by Trusel et al. (2010) who asserted

that the smallest particle size fraction (silt-clay) was the predominant sediment in suspension 470 m away from the glacier. Transportation and deposition of fine-grained sediment and mud from the glacier to distal locations is primarily driven by gravity currents (Curran et al., 2004) that can maintain concentrations of fine sediments greater than  $10 \text{ kg m}^{-3}$  in suspension (Mackiewicz et al., 1984).

Whereas suspended fine sand and coarse silt sink as single grains, the settling of finer silt and clay is affected by flocculation and the existence of aggregates (Syvitski, 1989; Curran et al., 2004). Flocculation is primarily dependent on sediment concentration (Mehta, 1986; Dyer, 1995; Hill et al., 1998, 2000; Shi and Zhou, 2004; Liu, 2005), but it is also influenced to a lesser extent by salinity, turbulence and other factors (Winterwerp, 2002; Dyer et al., 2002).

Field and laboratory studies of sedimentation from buoyant jets and plumes have been mainly focused on non-cohesive sediments (Carey et al., 1988; Sparks et al., 1991; Bursik, 1995; Ernst et al., 1996; Lane-Serff and Moran, 2005). Recently, Lane-Serff (2011) modeled the deposition of cohesive sediment from buoyant jets and found that the fall-speed decreases as the sediment load decreases. Lane-Serff also observed that the deposition rate was lower near the source but higher further away as more sediment remained in the current for longer distances.

Another process that has recently been shown to influence the sediment transport associated with buoyant plumes is convective sedimentation (McCool and Parsons, 2004). This is produced when the stratification hinders the descent speed of the sediment and, as a result, sediment concentrates along the pycnocline, until the region becomes gravitationally unstable and the inhomogeneities in the density field turn into convective cells (McCool and Parsons, 2004; Hoyal et al., 1999; Parsons and Garcia, 2001). Laboratory observations by Green (1987) about this "sediment fingering" showed that this process can be important especially in conditions of high sediment concentration, small particles and weak stratifica-

tion. Parsons et al. (2001) stated that this convection occurred even at sediment concentrations as low as  $1 \text{ kg m}^{-3}$ , and one consequence of the convective instability of the original hypopycnal plume was the generation of a bottom turbidity current, or hyperpycnal plume that moved at moderate speeds over the bottom.

There have been some modeling efforts to study the sedimentation process in glacial fjords. Mugford and Dowdeswell (2007) used a stratigraphic simulation model that could link the environmental and climatic conditions to the geological formation of distinctive glacial marine deposits in Kangerdlugssuaq Fjord (Greenland) and McBride Glacier (Alaska). More recently, Mugford and Dowdeswell (2011) used a jet model and could reproduce some important features of the sedimentation in McBride Glacier (Alaska).

Here we carry out a fundamental numerical study of fine sediment transport associated with buoyant discharges in glacial fjords, considering a range from buoyancy to momentum-dominated conditions. We hope to capture some basic understanding about the sediment transport in glacial fjords, using a simplified configuration that does not include ambient stratification, ocean currents, or ice processes.

### 3.3 Methods

#### 3.3.1 Sediment transport

In glacial fjords the freshwater source is a buoyant jet that usually enters the fjord at the base of the glacier, as subglacial discharges. The resulting vertical plume that flows along the glacier face has a typical horizontal length scale  $L \sim 1$  m, that is much smaller than the vertical scale of the plume which is roughly the fjord depth, i.e.  $H \sim 100$  m. The freshwater forcing in glacial fjords is, therefore, highly nonhydrostatic because  $H/L \gg 1$  (Marshall et al., 1997).

Most models used in oceanography consider the hydrostatic assumption which is justified when horizontal length scales  $L$  of the motion are several orders of magnitude larger than vertical length scales  $H$  (Cushman-Roisin, 1994). Hydrostatic models, however, are not suitable to simulate highly nonhydrostatic processes such as convection and high-frequency gravity waves (Marshall et al., 1997), shelf/slope convection, and buoyantly driven coastal jets (Gallacher et al., 2001; Shaw and Chao, 2006). Consequently, we used a nonhydrostatic model developed by Bourgault and Kelley (2004). The model used is a two dimensional, laterally averaged model and uses a finite difference scheme with a variable mesh  $z$ -coordinate  $C$ -grid. The model details and experimental configuration used here are described in Bourgault and Kelley (2004) and Salcedo-Castro et al. (2011b), respectively.

The numerical experiments were set in a two-dimensional configuration  $(x, z)$  representing a longitudinal section of a glacial fjord, and with freshwater forcing at the glacier face. The glacier was represented as a vertical wall with a no-slip boundary condition and the only forcing was a steady flow produced at the bottom open cells set through the glacier face. The total length of the numerical domain was 206 km and the total depth was  $H = 100$  m. The numerical grid has a constant vertical resolution of  $\Delta z = 1$  m. In the horizontal, the grid has a resolution of  $\Delta x = 1$  m for  $0 < x < 100$  m (i.e. the region of interest). For

$x > 100$  m the grid size increases linearly to a maximum of  $\Delta x = 5000$  m. The domain was made very long compared to the plume width such that the seaward boundary condition did not influence the results (Fig. 3.1).

The initial condition was set as still, uniform density ambient water and all simulations were run with a free surface and reached steady state in the region  $x < 100$  m before the freshwater front reached the seaward boundary.

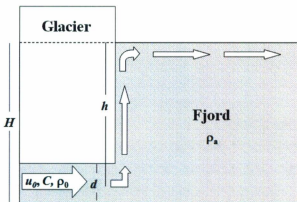


Figure 3.1: Schematic representation of a glacial fjord, showing parameters considered in numerical experiments.

The module for sediment transport in the model includes an equation for the advection-diffusion of sediment concentration,

$$\frac{\partial C}{\partial t} + u \frac{\partial C}{\partial x} + (w + w_s) \frac{\partial C}{\partial z} = \frac{\partial}{\partial x} \left( \kappa_x \frac{\partial C}{\partial x} \right) + \frac{\partial}{\partial z} \left( \kappa_z \frac{\partial C}{\partial z} \right), \quad (3.2)$$

where,  $C(x, z, t)$  is the sediment concentration,  $\kappa_x(x, z, t)$  is the coefficients of eddy diffusivity; and  $w_s$  is the sediment settling velocity. The initial diffusivity coefficient was set to  $\kappa_x = 1.0 \times 10^{-7} \text{ m}^2 \text{ s}^{-1}$ .

The following expression is included to account for the modification of the equation of

state for density by the presence of sediments (Wang et al., 2005):

$$\rho = \rho_w + \left(1 - \frac{\rho_w}{\rho_s}\right)C, \quad (3.3)$$

where  $\rho_w$  is the density of water and  $\rho_s$  is the density of sediment. Also, the model includes the following bottom boundary condition to represent the processes of resuspension and deposition (Partheniades, 1965; Kuijper et al., 1989; Markofsky and Westrich, 2007):

$$\kappa_c \frac{\partial C}{\partial z} - w_s C = E_b, \quad (3.4)$$

where:

$$E_b = \begin{cases} E_0 \left(\frac{|\tau_b|}{\tau_c} - 1\right) & \text{if } |\tau_b| > \tau_c \text{ (resuspension)} \\ C_b w_s \left(1 - \frac{|\tau_b|}{\tau_c}\right) & \text{if } |\tau_b| < \tau_c \text{ (deposition)} \end{cases} \quad (3.5)$$

Here,  $E_b$  is the bottom sediment flux,  $E_0$  is the erosion coefficient,  $C_b$  is the sediment concentration at the bottom layer; and  $\tau_c$  is the critical stress for resuspension and deposition (McAnally and Mehta, 2001; van Rijn, 2007). The choice of parameters used here is shown in Table 3.1.

Table 3.1: Parameters used for sediment transport in the model

Parameter	Value
$\rho_s$ (kg m <sup>-3</sup> )	2,650
$\rho_w$ (kg m <sup>-3</sup> )	1,000
$w_0$ (m s <sup>-1</sup> )	0.0001
$E_0$ (kg m <sup>-2</sup> s <sup>-1</sup> )	0.0001
$\tau_c$ (Pa)	0.3

### 3.3.2 Flocculation

All runs considered the sediment grain fraction that predominates in glacial fjords, which is in the range of the silt-clay fraction (mud) (Table 3.2). Thus we chose a cohesive sediment whose representative particle settling velocity was roughly  $1.0 \times 10^{-5} \text{ m s}^{-1}$  (very fine silt-coarse clay with grain density of  $\sim 2650 \text{ kg m}^{-3}$ ). Therefore, it was necessary to represent the process of flocculation in the model.

Table 3.2: Typical values of sediment concentration and grain size found in glacial fjords

Location	Reference	Concentration range (kg m <sup>-3</sup> )	Size range
Arthur Harbor, Antarctica	Ashley and Smith (2000)	0.003 - 0.035	clay/silt (30:60)
MacBride Glacier, Alaska	Cowan and Powell (1990)	0.45 - 0.50	
MacBride Glacier, Alaska	Cowan et al. (1988)	0.5 - 2	99.6% < 63µm
Hubbard Glacier	Curran et al. (2004)	0.01 - 0.035	
Cierva, Brialmont, Lester Cove, Antarctica	Domack and Williams (1990)	0.0006 - 0.008	
Brialmont Cove, Antarctica	Domack et al. (1994)	0.00075 - 0.0041	2 - 10µm
Watts Glacier and Coronation-Maktak fjords	Dowdeswell (1986)		< 4µm
Spitsbergen	Elverhøi et al. (1983)	0.02 - 0.5	
Kongsfjorden, Spitsbergen, Norway	Fetzer et al. (2002)		90% clay/silt (50:50)
Coronation Fjord, Baffin Island	Gilbert (1982)		30 - 100µm
Pangnirtung Fjord	Gilbert (1978)		65 - 90% clay/silt
Hornsund Fjord, Spitsbergen	Görlich et al. (1987)	0.01 - 1	
Itirbiling Fjord, Baffin Island	Hein and Syvitski (1992)		sand/mud (50:50)
Blue Fjord, Alaska	Hoskin et al. (1978)	0.01 - 0.3	46 - 53µm
Muir Inlet, Alaska	Mackiewicz et al. (1984)		65 - 90% 4 - 16µm
Nordostlandet tidewater ice cap, Svalbard	Pfirman and Solheim (1989)	0.001 - 0.028	
Lange Glacier, Antarctica	Pichlmaier et al. (2004)	0.007 - 0.011	
Martel Inlet, Antarctica	Pichlmaier et al. (2004)	0.01 - 0.015	
Kongsfjorden, Svalbard, Norway	Svendsen et al. (2002)	<0.02 - 0.34	
Coronation Fjord, Baffin Island	Syvitski (1989)	0.01 - >0.120	
Billefjorden, Svalbard	Szczucinski et al. (2009)		> 90% clay/silt (50:50)
Kongsfjorden, Svalbard	Trusel et al. (2010)	0.008 - 0.157	
Kongsfjorden, Svalbard	Zaborska et al. (2006)	> 0.3	> 90% clay/silt (10:90)
Kongsfjorden, Svalbard	Zajęczkowski (2008)	0.35 - 0.46	

Table 3.3: Parameters used for flocculation in the model

Parameter	Value
$k_1$	0.14
$n$	1.04
$k_2$	0.0001
$w_{30}$ (m s <sup>-1</sup> )	0.0026
$\beta$	4.65

To represent flocculation, we used the well-known power law relationship between sediment concentration and settling velocity (Mehta, 1986) (eq. 3.6b), modified to account for reduced settling velocity caused by high sediment concentrations (Richardson and Zaki, 1954; Mehta, 1986; Puls et al., 1988) (eq. 3.6c):

$$w_s = \begin{cases} w_0 & \text{if } C \leq 8.6 \times 10^{-3} \text{ kg m}^{-3} & (3.6a) \\ k_1 C^n & \text{if } 8.6 \times 10^{-3} < C \leq 1.7 \text{ kg m}^{-3} & (3.6b) \\ w_{30} (1 - k_2 C)^\beta & \text{if } C > 1.7 \text{ kg m}^{-3} & (3.6c) \end{cases}$$

The setting for flocculation is shown in Table 3.3. The parameters set in Table 3.3 result in a maximal settling velocity of  $2.4 \times 10^{-3} \text{ m s}^{-1}$ , which is in the range observed in the field (Hill et al., 1998; Shi and Zhou, 2004). The dependence of settling velocity on sediment concentration is linear up to a concentration of  $1 \text{ kg m}^{-3}$  (Fig. 3.2).

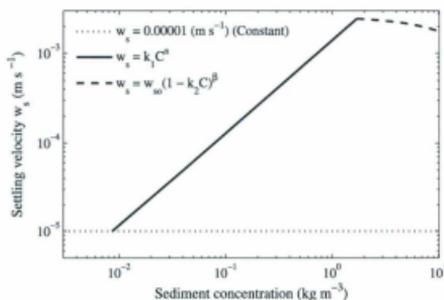


Figure 3.2: Settling velocity as function of sediment concentration.

Experiments covering a range from buoyancy to jet dominated conditions were run. These experiments encompassed a range of  $Fr$  between 0.01 and 3.2 and are summarized in Fig. 3.3. Four sediment concentrations were set: 0.1, 0.1, 1, and  $10 \text{ kg m}^{-3}$ . The upper end of this range of concentrations was set according to observations made by some authors (Gilbert, 1983; Mackiewicz et al., 1984; Gilbert et al., 2002).

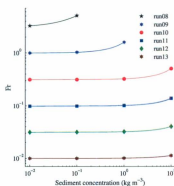


Figure 3.3: Effect of sediment concentration on  $Fr$  number.

## 3.4 Results

### 3.4.1 Plume sediment concentration

All experiments exhibited similar flow patterns: a buoyant jet issuing horizontally from the tunnel opening, a vertical plume rising attached to the "wall" that produced a lifting of the sea surface when reaching the surface and a gravity surface current that set an estuarine circulation (Fig. 3.4). There is a clear difference between momentum-dominated and buoyancy-dominated runs. The momentum-dominated runs showed a jet spreading horizontally on the bottom for a distance of some meters until a balance is reached as momentum is lost and buoyancy forces the jet to veer up and back to the wall to rise as a vertical plume. On the other hand, the buoyancy-dominated runs went up immediately after leaving the tunnel opening.

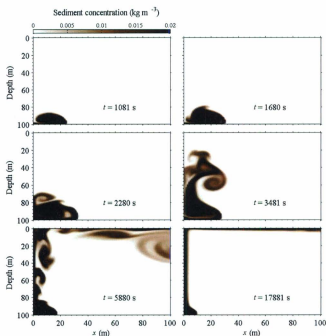


Figure 3.4: Typical sequence of sediment concentration in a momentum-dominated jet issuing into the ambient denser water (run08, initial jet sediment concentration:  $0.1 \text{ kg m}^{-3}$ ).

Flocculation did not produce any noticeable deviation of the description above for concentrations lower than  $1 \text{ kg m}^{-3}$ . When the initial jet sediment concentration was  $10 \text{ kg m}^{-3}$ , the experiments exhibited a different pattern. After apparently having reached steady state, some sediment commenced to settle through the water column in the far field (between 1500 and 5000 meters away of the glacier)(Fig. 3.5), in the form of finger-like extensions that came off the surface layer. This convective transport was preceded by subsurface higher sediment concentrations, between  $0.3 - 0.4 \text{ kg m}^{-3}$ , and reached velocities higher than  $1.0 \times 10^{-2} \text{ m s}^{-1}$  and involved deposition rates between  $5.0 \times 10^{-4}$  and  $1.0 \times 10^{-3} \text{ kg m}^{-2}\text{s}^{-1}$ .

In contrast, deposition rates between  $1.0$  and  $8.0 \times 10^{-4} \text{ kg m}^{-2}\text{s}^{-1}$  were observed above the bottom. As sediment settled through the water column, it was carried back to the glacier by the landward lower estuarine current and re-entrained into the vertical and horizontal plumes (Fig. 3.6). This process was also observed in run # 09, with an initial jet sediment concentration of  $1 \text{ kg m}^{-3}$ .

Vertical profiles of sediment concentration for the runs with an initial jet sediment concentration of  $10 \text{ kg m}^{-3}$  were obtained at a distance  $10 d$  away of the glacier (Fig. 3.7). The sediment concentration at the surface is higher from run10 to run 13 (increasing buoyancy-dominance) and this causes a progressive weakening of the gradient at the interface. A decrease of the sediment concentration through the water column from run10 to run 13 is seen too. It is also possible to observe the lutocline above the bottom.

Density was affected by the presence of sediment in the far field and this can be seen in Fig. 3.8. The sediment concentration increased and formed a thin layer of higher concentration at the base of the horizontal buoyant plume. After some time, this thin layer collapsed and sediment settled through the water column, driven by convective mixing, and forming clouds of sediment that are transported back to the glacier. This effect of sediment on the density was also observed in the near field (Fig. 3.9).

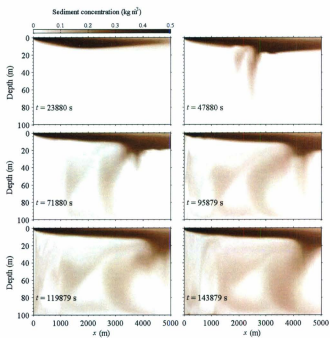


Figure 3.5: Sequence of sediment concentration in the gravity plume spreading at the surface and settling of sediment in the far field (run10, initial jet sediment concentration:  $10 \text{ kg m}^{-3}$ ).

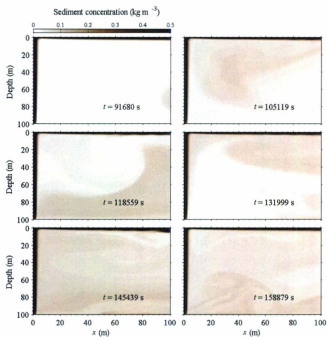


Figure 3.6: Sequence of sediment concentration in the gravity plume spreading at the surface and settling of sediment in the near field (run10, initial jet sediment concentration:  $10 \text{ kg m}^{-3}$ ).

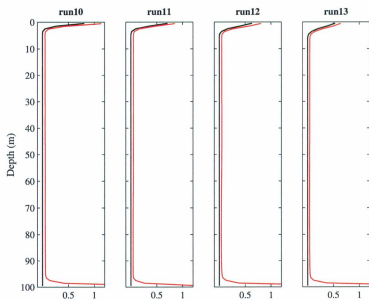


Figure 3.7: Sediment concentration profiles (red) taken at a distance equivalent to  $10 d$ , where  $d$  is the opening diameter (Initial jet sediment concentration:  $10 \text{ kg m}^{-3}$ ). Experiments without flocculation are included (black lines) for comparison.

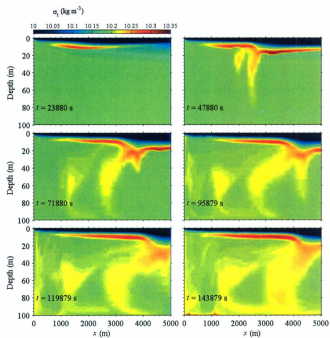


Figure 3.8: Sequence of density anomaly field and changes associated with settling of sediment in the far field (run10, initial jet sediment concentration:  $10 \text{ kg m}^{-3}$ ).

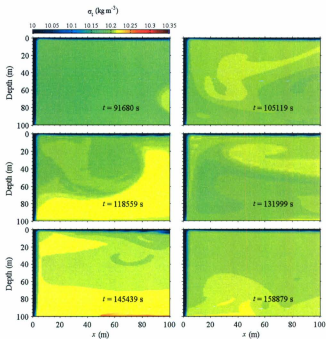


Figure 3.9: Sequence of density anomaly field and changes associated with settling of sediment in the near field (run10, initial jet sediment concentration:  $10 \text{ kg m}^{-3}$ ).

The maximum sediment concentration of the surface plume through a vertical cross-section at distance  $10d$  from the glacier was extracted and compared to the input concentration. The same analysis was done for a horizontal cross-section taken through the vertically rising plume at a distance  $10d$  from the bottom. The sediment concentration, nondimensionalized with the initial jet sediment concentration, is lower as we move from momentum dominated (high Fr) to buoyancy dominated (low Fr) conditions in the vertical (Fig. 3.10(a)) and horizontal plumes (Fig. 3.10(b)). Low sediment concentrations at the discharge ( $10^{-2} - 10^{-1} \text{ kg m}^{-3}$ ) primarily affected the momentum-dominated experiments

as they showed a rapid increase as response to these low concentrations. On the other hand, when the discharge carried higher sediment concentrations ( $1 - 10 \text{ kg m}^{-3}$ ) it was possible to observe an increasing trend in buoyancy-dominated runs, especially at higher concentrations. This response, however, is less intense as buoyancy becomes relatively more important (decreasing  $Fr$ ).

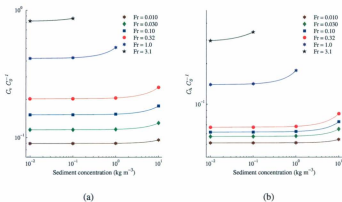


Figure 3.10: Effect of sediment concentration on the vertical (a) and horizontal (b) plume concentration for different  $Fr$  numbers at a distance equivalent to  $10 d$ , where  $d$  is the opening diameter.

The response to increasing sediment concentrations was also assessed in terms of the upward sediment transport by the vertical plume. The sediment transport was computed through the following equation:

$$F = \int_{x=0}^{x=P_{edge}} C w dx, \quad (3.7)$$

where  $P_{edge}$  was defined as the seaward limit where  $w = 0.01w_{max}$ .

The computed sediment fluxes increase as buoyancy increases (from run08 to run13)(Fig. 3.11). Runs 08 and 09 (momentum-dominated) showed a slight increase of sediment transport in

spite of their more accentuated velocity drop because they kept relatively high sediment concentrations with respect to the sediment concentration at the initial jet coming out from the tunnel opening.

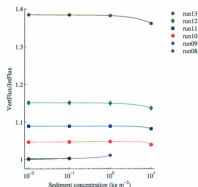


Figure 3.11: Vertical sediment flux (nondimensionalized with the initial jet sediment flux) computed at  $10d$ , where  $d$  is the opening diameter.

### 3.4.2 Plume velocity

Momentum-dominated runs were more sensitive to the presence of sediments (Figs. 3.12). Under the effect of the sediment concentration, the vertical plume velocity rapidly decays in momentum-dominated conditions. In buoyancy-dominated experiments however this deceleration is noticeable only at high sediment concentrations (Figs. 3.12(a)). A similar pattern was observed in the maximum velocity of the surface plume, at a distance equivalent to  $10d$  away from the glacier (Figs. 3.12(b)).

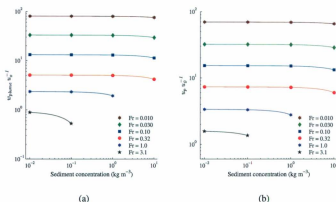


Figure 3.12: Effect of sediment concentration on the vertical (a) and horizontal (b) plume velocity for different Fr numbers at a distance equivalent to  $10d$ , where  $d$  is the opening diameter.

### 3.4.3 Plume dilution

A dilution factor (Anwar, 1973; Lee and Lee, 1998; Chen and Rodi, 1980; Huai et al., 2010) was computed to evaluate the degree of mixing along the vertical and horizontal plumes, which was defined as:

$$S = \frac{\rho_a - \rho_0}{\rho_a - \rho_p}, \quad (3.8)$$

where  $\rho_p$  is the plume density, at a distance equivalent to  $10d$  above the tunnel opening for the vertical plume and  $10d$  away from the glacier for the surface gravity plume.

Similar to the case of velocities the experiments showed an increasing plume dilution as buoyancy becomes more important (decreasing Fr) (Figs. 3.13). The vertical (Figs. 3.13(a)) and horizontal (Figs. 3.13(b)) plume dilution was relatively unaffected by low sediment concentrations, with exception of the momentum-dominated runs (run08 and run09). As

the jet sediment concentration increases, the buoyancy-dominated experiments showed a decrease in their dilution capacity. This reduction in dilution, however, is lower as the experiments are in the extreme of buoyancy-dominance.

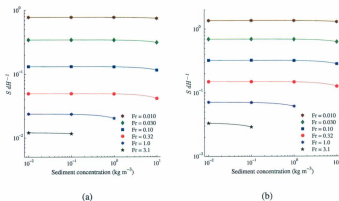


Figure 3.13: Effect of sediment concentration on the vertical (a) and horizontal (b) plume dilution for different Fr numbers at a distance equivalent to  $10d$ , where  $d$  is the opening diameter.

### 3.5 Discussion

The addition of sediment produces a decrease in buoyancy and, consequently, a higher Fr number. This is relevant in glacial fjords because, as Salcedo-Castro et al. (2011b) pointed out, the estuarine circulation is primarily driven by the plume buoyancy, with the plume momentum playing a secondary role. As observed in the variations of velocity, sediment concentration and dilution, however, buoyancy still remains as the main factor controlling the fine sediment transport and sediment produces significant changes only at relatively high concentrations.

The experiments showed that fine sediment can be transported a relatively long distance away of the glacier by the horizontal buoyant plume and the sediment concentration is progressively diluted by entrainment before starting to settle through the water column. Similarly, Lane-Serff (2011) observed a lower deposition rate of cohesive sediment near the origin (compared to non-cohesive sediment) but became higher further away from the source (as more sediment remains in the current for longer distances).

All experiments with jet sediment concentration of  $10 \text{ kg m}^{-3}$  exhibited higher subsurface sediment concentrations at the base of the horizontal plume in the far field. This higher sediment concentration led to an instability and finally a convective transport of sediment downward through the water column. This description seems to agree well with the explanation provided by Carey et al. (1988) who asserted that the downward flux of sediment through the water column could be caused by the re-entrainment of sedimenting particles in the fluid around the plume that increase the particle concentration of the plume margins so that it would have a density greater than either the ambient fluid or the plume interior.

The convective transport of sediment down through the water column observed in our experiments had higher vertical velocities than those caused by flocculation. This pattern was similar to the description given by McCool and Parsons (2004), who observed convec-

tive plumes that dominated sedimentation and had vertical velocities of 1-2 cm s<sup>-1</sup>, two orders of magnitude larger than those predicted by Stokes settling of the constituent particles. Also, surface plume concentrations as low as 380 mg L<sup>-1</sup> (0.38 kg m<sup>-3</sup>) were documented to support robust mixing-induced convective sedimentation (McCool and Parsons, 2004), which is in the same range observed in this study.

The process of sediment being carried back and re-entrained into the vertical and horizontal plumes has been described for non-cohesive sediments by other investigators. In plumes with concentrations greater than 10 g L<sup>-1</sup>, Carey et al. (1988) observed the generation of dilute downward moving flows along the side of the vertical plume. Sparks et al. (1991) described an outer region where sediment falls out from the base of a horizontal turbulent gravity current and is drawn back towards the plume by a net inflow caused by the entrainment of ambient fluid as the plume rises. Ernst et al. (1996) also observed that the re-entrainment was most vigorous in runs with relatively fine-grained particles and buoyant plumes or strong jets. More recently, Cuthbertson and Davies (2008) described a tendency of settling of non-cohesive particles to be drawn back towards the margins of the rising buoyant jet and this return flow could be sufficiently strong to re-entrain depositing particles into the rising buoyant jet. Besides, Cuthbertson et al. (2008) defined a critical distance within which particles would be re-entrained back into the rising buoyant jet, whereas those settling beyond this distance will deposit to the bed. Our results, however, showed a combination of these processes where sediment is transported from the far field back to the vertical plumes and, at the same time, part of the sediment is being deposited on the bed.

The experiments with initial sediment concentrations of 10 kg m<sup>-3</sup> in the issuing jet had sediment concentrations at the surface plume between 0.7 - 1 kg m<sup>-3</sup> which yield settling floc velocities of 1 - 1.4 mm s<sup>-1</sup>. This range is similar to what has been observed in fjords and other estuaries by some authors. Hill et al. (1998) found that the predicted settling velocity of a 1 mm diameter floc is 1.5 mm s<sup>-1</sup>. Shi and Zhou (2004) calculated settling

velocities from 0.4 to 4.1 mm s<sup>-1</sup> for the point-sampled data set, and from 1.0 to 3.0 mm s<sup>-1</sup> for an acoustically measured data set.

Despite the good representation of fine sediment transport by the model, there are other processes not included and that could predominate during certain stages and in some regions of the jet and vertical and horizontal plumes. Verney et al. (2009) demonstrated that turbulent intensity is one of the main determining factors of maximum floe size. In this sense, Pejrup and Mikkelsen (2010) has shown that the with the inclusion of turbulence, an improvement of up to 72% has been found in explaining the variation in settling velocity. In this sense, Domack et al. (1994) stated that turbulent mixing near the seafloor can play an important role in the transport and break-up of floccules.

In our simulations, the background environment was considered motionless, without wind or tides that produce background turbulence. This is justified for high latitude systems where the tidal range is narrow when compared to other estuaries. In this sense, wave-associated resuspension is not considered important either, as we represented a glacial fjord adjacent to a tidewater outlet glacier where shallow areas and tidal flats are practically inexistent. Further studies should consider the inclusion of turbulence and mixing associated with waves, which is expected to produce somewhat different results. Simulations with realistic tidal forcing and stratified conditions are left to further studies.

### 3.6 Conclusion

Momentum-dominated conditions are more sensitive than buoyancy-dominated conditions to the presence of sediment in the buoyant jet discharging into the ambient water. Therefore this type of experiments shows response at even low sediment concentrations. On the other hand, buoyancy-dominated experiments exhibited noticeable changes only at high sediment concentrations and this response was less intense as buoyancy increased ( $Fr$  becoming smaller).

Cohesive sediments do not settle in the near field but it is transported to the far field and settle there. Then it is carried back to the glacier and re-entrained into the vertical and horizontal plumes.

The density field is affected by the presence of sediment, as instabilities were produced by higher subsurface sediment concentrations observed at the interface between the upper and lower layer, and clouds of this denser water (and sediment) go down convectively through the water column.

Convective sedimentation proved to be a more efficient mechanism of vertical sediment transport of fine sediment, compared to individual particles settling and flocculation.

### 3.7 References

- Anwar, H. O., 1973. Two-dimensional buoyant jet in a current. *Journal of Engineering Mathematics* 7 (4), 297 – 311.
- Apollonio, S., 1973. Glaciers and nutrients in arctic seas. *Science* 180 (4085), 491 – 493.
- Ashley, G. M., Smith, N. D., 2000. Marine sedimentation at a calving glacier margin. *Geological Society of America Bulletin* 112 (5), 657–667.

- Bourgault, D., Kelley, D. E., 2004. A laterally averaged nonhydrostatic ocean model. *Journal of Atmospheric and Oceanic Technology* 21, 1910–1924.
- Bursik, M. I., 1995. Theory of the sedimentation of suspended particles from fluvial plumes. *Sedimentology* 42, 831–838.
- Carey, S. N., Sigurdsson, H., Sparks, R. S. J., 1988. Experimental studies of particle-laden plumes. *Journal of Geophysical Research* 93 (B12), 15,314–15,328.
- Carney, D., Oliver, J. S., Armstrong, C., 1999. Sedimentation and composition of wall communities in Alaskan fjords. *Polar Biology* 22, 38 – 49.
- Chen, C. J., Rodi, W., 1980. *Vertical turbulent buoyant jets – A review of experimental data*. Pergamon Press.
- Cowan, E. A., Powell, R. D., 1990. Suspended sediment transport and deposition of cyclically interlaminated sediment in a temperate glacial fjord, Alaska, U.S.A. Geological Society, London, Special Publications 53, 75–89.
- Cowan, E. A., Powell, R. D., Smith, N. D., 1988. Rainstorm-induced event sedimentation at the tidewater front of a temperate glacier. *Geology* 16, 409–412.
- Curran, K., Hill, P., Milligan, T., Cowan, E., Syvitski, J., Konings, S., 2004. Fine-grained sediment flocculation below the Hubbard Glacier meltwater plume, Disenchantment Bay, Alaska. *Marine Geology* 203, 83–94.
- Cushman-Roisin, B., 1994. *Introduction to geophysical fluid dynamics*. Prentice Hall.
- Cuthbertson, A. J. S., Davies, P. A., 2008. Deposition from particle-laden, round, turbulent, horizontal, buoyant jets in stationary and coflowing receiving fluids. *Journal of Hydraulic Engineering* 134 (4), 390–402.

- Cuthbertson, Alan J. S. and Apsley, D. D., Davies, P. A., Lipari, G., Stansby, P. K., 2008. Deposition from particle-laden, plane, turbulent, buoyant jets. *Journal of Hydraulic Engineering* 134 (8), 1110–1122.
- Domack, E. W., Foss, D. J. P., Syvitski, J. P. M., McClennen, C. E., 1994. Transport of suspended particulate matter in an Antarctic fjord. *Marine Geology* 121, 161–170.
- Domack, E. W., Williams, C. R., 1990. Fine structure and suspended sediment transport in three Antarctic fjords. *Antarctic Research Series* 50, 71–89.
- Dowdeswell, J. A., 1986. The distribution and character of sediments in a tidewater glacier, Southern Baffin Island, N.W.T., Canada. *Arctic and Alpine Research* 18 (1), 45–56.
- Dyer, K. R., 1995. Sediment transport processes in estuaries. In: Perillo, G. M. E. (Ed.), *Geomorphology and Sedimentology of Estuaries. Developments in Sedimentology*, 53. Elsevier, pp. 423–449.
- Dyer, K. R., Bale, A. J., Christie, M. C., Feates, N., Jones, S., Manning, A. J., 2002. The turbidity maximum in a mesotidal estuary, the Tamar estuary, UK: II. the flocc properties. In: Winterwerp, J. C., Kranenburg, C. (Eds.), *Fine sediment dynamics in the marine environment*. Elsevier, pp. 219–232.
- Elverhøi, A., Lønne, Ø., Seland, R., 1983. Glaciomarine sedimentation in a modern fjord environment, Spitsbergen. *Polar Research* 1 (2), 127–149.
- Ernst, G. G. J., Sparks, R. S. J., Carey, S. N., Bursik, M. I., 1996. Sedimentation from turbulent jets and plumes. *Journal of Geophysical Research* 101 (B3), 5575–5589.
- Etherington, L. L., Hooge, P. N., Hooge, E. R., Hill, D. F., 2007. Oceanography of Glacier Bay, Alaska: Implications for biological patterns in a glacial fjord estuary. *Estuaries and Coasts* 30 (6), 927–944.

- Fetzer, I., Lønne, O. J., Pearson, T., 2002. The distribution of juvenile benthic invertebrates in an Arctic glacial fjord. *Polar Biology* 25, 303–315.
- Gallacher, P. C., Piacsek, S., Dietrich, D., 2001. Hydrostatic and nonhydrostatic simulations of buoyantly driven coastal jets. In: Spaulding, M. L. (Ed.), *Proceedings of the Seventh International Conference, November 5-7, 2001, St. Petersburg, Florida*. pp. 204–214.
- Gilbert, R., 1978. Observations on oceanography and sedimentation at Pangnirtung fjord, Baffin Island. *Maritime Sediments* 14 (1), 1–9.
- Gilbert, R., 1982. Contemporary sedimentary environments on Baffin Island, N.W.T., Canada: Glaciomarine processes in fiords of Eastern Cumberland Peninsula. *Arctic and Alpine Research* 14 (1), 1–12.
- Gilbert, R., 1983. Sedimentary processes of Canadian Arctic fiords. *Sedimentary Geology* 36, 147–175.
- Gilbert, R., Nielsen, N., Möller, H., Desloges, J. R., Rasch, M., 2002. Glaciomarine sedimentation in Kangerdluk (Disko Fjord), West Greenland, in response to a surging glacier. *Marine Geology* 191, 1–18.
- Görlich, K., Węstawski, J. M., Zajączkowski, M. J., 1987. Suspension settling effect on macrobenthos biomass distribution in the Hornsund fjord, Spitsbergen. *Polar Research* 5, 175–192.
- Green, T., 1987. The importance of double diffusion to the settling of suspended material. *Sedimentology* 34 (2), 319–331.
- Hein, F. J., Syvitski, J. P. M., 1992. Sedimentary environments and facies in an arctic basin, Itirbilung Fiord, Baffin Island, Canada. *Sedimentary Geology* 81, 17–45.

Hill, P. S., Milligan, T. G., Geyer, W. R., 2000. Controls on effective settling velocity of suspended sediment in the Eel River flood plume. *Continental Shelf Research* 20, 2095–2111.

Hill, P. S., Syvitski, J. P., Cowan, E. A., Powell, R. D., 1998. In situ observations of floe settling velocities in Glacier Bay, Alaska. *Marine Geology* 145, 85–94.

Hooge, P. N., Hooge, E. R., 2002. Fjord oceanographic processes in glacier bay, alaska. USGS - Alaska Science Center, 144 pp.

Hop, H., Pearson, T., Hegseth, E. N., Kovacs, K. M., Wiencke, C., Kwasniewski, S., Eliane, K., Mehlum, F., Gulliksen, B., Wlodarska-Kowalczyk, M., Lydersen, C., Weslawski, J. M., Cochrane, S., Gabrielsen, G. W., Leakey, R. J. G., Lønne, O. J., Zajaczkowski, M., Falk-Petersen, S., Kendall, M., Wängberg, S.-Å., Bischof, K., Voronkov, A. Y., Kovaltchouk, N. A., Wiktor, J., Poltermann, M., Di Prisco, G., Papucci, C., Gerland, S., 2002. The marine ecosystem of Kongsfjorden, Svalbard. *Polar Research* 21 (1), 167–208.

Hoskin, C. M., Burrell, D. C., Freitag, G. R., 1978. Suspended sediment dynamics in Blue Fjord, Western Prince William Sound, Alaska. *Estuarine and Coastal Marine Science* 7, 1–16.

Hoyal, D. C. J. D., Bursik, M. I., Atkinson, J. F., 1999. The influence of diffusive convection on sedimentation from buoyant plumes. *Marine Geology* 159, 205–220.

Huai, W., Li, Z., Qian, Z., Zeng, Y., Han, J., 2010. Numerical simulation of horizontal buoyant wall jet. *Journal of Hydrodynamics* 22, 58–65.

Kuijper, C., Cornelisse, J. M., Winterwerp, J. C., 1989. Research on erosive properties of cohesive sediments. *Journal of Geophysical Research* 94, 14,341–14,350.

- Lane-Serff, G. F., 2011. Deposition of cohesive sediment from turbulent plumes, gravity currents and turbidity currents. *Journal of Hydraulic Engineering (In Press)*, doi:10.1061/(ASCE)HY.1943-7900.0000463.
- Lane-Serff, G. F., Moran, T. J., 2005. Sedimentation from buoyant jets. *Journal of Hydraulic Engineering* 131 (3), 166–174, doi:10.1061/(ASCE)0733-9429(2005)131:3(166).
- Lee, W. T., Lee, J. H. W., 1998. Effect of lateral confinement on initial dilution of vertical round buoyant jet. *Journal of Hydraulic Engineering* 124, 263–279.
- Liu, W.-C., 2005. Modeling the influence of settling velocity on cohesive sediment transport in Tanshui River estuary. *Environmental Geology* 47, 535–546, doi:10.1007/s00254-004-1176-z.
- Mackiewicz, N. E., Powell, R. D., Carlson, P. R., Molnia, B. F., 1984. Interlaminated ice-proximal glacial marine sediments in Muir Inlet, Alaska. *Marine Geology* 57, 113–147.
- Markofsky, M., Westrich, B., 2007. Transport modeling. In: Westrich, B., Ulrich, F. (Eds.), *Sediment Dynamics and Pollutant Mobility in Rivers. An Interdisciplinary Approach*. Springer, pp. 117–169.
- Marshall, J., Hill, C., Perelman, L., Adcroft, A., 1997. Hydrostatic, quasi-hydrostatic, and nonhydrostatic ocean modeling. *Journal of Geophysical Research* 102 (C3), 5733–5752.
- McAnally, W. H., Mehta, A. J., 2001. Seasonal variability of sediment erodibility and properties on a macrotidal mudflat, Peterstone Wentloogw, Severn estuary, UK. In: Mitchener, H. J., O'Brien, D. J. (Eds.), *Coastal and estuarine fine sediment processes*. Elsevier, pp. 301–322.
- McCool, W. W., Parsons, J. D., 2004. Sedimentation from buoyant fine-grained suspensions. *Continental Shelf Research* 24, 1129–1142, doi:10.1016/j.csr.2004.03.009.

Mehta, A. J., 1986. Characterization of cohesive sediment properties and transport processes in estuaries. In: Mehta, A. J. (Ed.), *Estuarine cohesive sediment dynamics*. Lecture notes on coastal and estuarine studies. Springer-Verlag, pp. 290–325.

Mugford, R. I., Dowdeswell, J., 2007. Numerical modelling of glacial marine sedimentation from tidewater glaciers: iceberg-rafted vs meltwater plume deposition. *Geophysical Research Abstracts* 9 (10297).

Mugford, R. I., Dowdeswell, J. A., 2011. Modeling glacial meltwater plume dynamics and sedimentation in high-latitude fjords. *Journal of Geophysical Research* 116 (F01023), doi:10.1029/2010JF001735.

Parsons, J. D., Bush, J. W. M., Syvitsky, J. P. M., 2001. Hyperycnal plume formation from riverine outflows with small sediment concentrations. *Sedimentology* 48, 465–478.

Parsons, J. D., Garcia, M. H., 2001. Enhanced sediment scavenging due to double-diffusive convection. *Journal of Sedimentary Research* 70 (1), 47–52.

Partheniades, E., 1965. Erosion and deposition of cohesive soils. *Journal of the Hydraulics Division* 91, 105–139.

Pejrup, M., Mikkelsen, O. A., 2010. Factors controlling the field settling velocity of cohesive sediment in estuaries. *Estuarine, Coastal and Shelf Science* 87, 177–185.

Pfirman, S. L., Solheim, A., 1989. Subglacial meltwater discharge in the open-marine tidewater glacier environment: Observations from Nordaustlandet, Svalbard Archipelago. *Marine Geology* 86, 265–281.

Pichlmaier, M., Aquino, F. E., Da-Silva, C. S., Braun, M., 2004. Suspended sediments in Admiralty Bay, King George Island (Antarctica). *Pesquisa Antartica Brasileira* 4, 77–85.

Powell, R. D., 1990. Glacimarine processes at grounding-line fans and their growth to ice-contact deltas. In: Dowdeswell, J. A., Scourse, J. D. (Eds.), *Glacimarine Environments: Processes and Sediments*. Geological Society Special Publication. Vol. 53. The Geological Society, pp. 53–73.

Puls, W., Kuehl, H., Heymann, K., 1988. Settling velocity of mud flocs: results of field measurements in the Elbe and the Wesser estuary. In: Dronkers, J., van Leussen, W. (Eds.), *Physical Processes in Estuaries*. Springer-Verlag, pp. 404–424.

Richardson, J. F., Zaki, W. N., 1954. The sedimentation of a suspension of uniform spheres under conditions of viscous flow. *Chemical Engineering Science* 3 (2), 65–73.

Russell, H., Arnott, R., 2003. Hydraulic-jump and hyperconcentrated-flow deposits of a glaciogenic subaqueous fan: Oak Ridges Moraine, southern Ontario, Canada. *Journal of Sedimentary Research* 73 (6), 887–905.

Salcedo-Castro, J., Bourgault, D., Bentley, S., deYoung, B., 2011a. Modeling ice-proximal fine sediment transport associated with a subglacial buoyant jet in glacial fjords: A fundamental approach. *Marine Geology* (*Submitted*).

Salcedo-Castro, J., Bourgault, D., deYoung, B., 2011b. Circulation induced by subglacial discharge in glacial fjords: Results from idealized numerical simulations. *Continental Shelf Research* 31, 1396–1406.

Sexton, D. J., Dowdeswell, J. A., Solheim, A., Elverhøi, A., 1992. Seismic architecture and sedimentation in northwest Spitsbergen fjords. *Marine Geology* 103, 53–68.

Shaw, P.-T., Chao, S.-Y., 2006. A nonhydrostatic primitive-equation model for studying small-scale processes: An object-oriented approach. *Continental Shelf Research* 26, 1416–1432.

- Shi, Z., Zhou, H. J., 2004. Controls on effective settling velocities of mud flocs in the Changjiang Estuary, China. *Hydrological Processes* 18, 2877–2892.
- Sparks, R. S. J., Carey, S. N., Sigurdsson, H., 1991. Sedimentation from gravity currents generated by turbulent plumes. *Sedimentology* 38, 839–856.
- Svendsen, H., Beszczynska-Møller, A., Hagen, J. O., Lefauconnier, B., Tverberg, V., Gerland, S., Børre-Orbæk, J., Bischof, K., Papucci, C., Zajaczkowski, M., Azzolini, R., Bruland, O., Wiencke, C., Winther, J. G., Dallmann, W., 2002. The physical environment of Kongsfjorden-Krossfjorden, an Arctic fjord system in Svalbard. *Polar Research* 21, 133–166.
- Syvitski, J. P. M., 1989. On the deposition of sediment within glacier-influenced fjords: Oceanographic controls. *Marine Geology* 85, 301–329.
- Syvitski, J. P. M., Murray, J. W., 1981. Particle interaction in fjord suspended sediment. *Marine Geology* 39, 215–242.
- Szczuciński, W., Zajaczkowski, M., Scholten, J., 2009. Sediment accumulation rates in subpolar fjords-Impact of post-Little Ice Age glaciers retreat, Billefjorden, Svalbard. *Estuarine, Coastal and Shelf Science* 85, 345–356.
- Trusel, L. D., Powell, R. D., Cumpston, R. M., Brigham-Grette, J., 2010. Modern glacial-marine processes and potential future behaviour of Kronebreen and Kongsvegen polythermal tidewater glaciers, Kongsfjorden, Svalbard. In: Howe, J. A., Austin, W. E. N., Forwick, M., Paetzel, M. (Eds.), *Fjord Systems and Archives*. Vol. 344. Geological Society, London, Special Publications, pp. 89–102.
- van Rijn, L. C., 2007. Unified view of sediment transport by currents and waves. I: Initiation of motion, bed roughness, and bed-load transport. *Journal of Hydraulic Engineering* 133 (6), 649–667.

Verney, R., Lafite, R., Brun-Cottan, J.-C., 2009. Flocculation potential of estuarine particles: The importance of environmental factors and of the spatial and seasonal variability of suspended particulate matter. *Estuaries and Coasts* 32, 678–693.

Wang, X. H., Byun, D. S., Wang, X. L., Chod, Y. K., 2005. Modelling tidal currents in a sediment stratified idealized estuary. *Continental Shelf Research* 25, 655–665.

Winterwerp, J. C., 2002. On the flocculation and settling velocity of estuarine mud. *Continental Shelf Research* 22, 1339–1360.

Zaborska, A., Pempkowiak, J., Papucci, C., 2006. Some sediment characteristics and sedimentation rates in an Arctic fjord (Kongsfjorden, Svalbard). *Środkowo-Pomorskie Towarzystwo Naukowe Ochrony Środowiska* 8 (80-97).

Zajęczkowski, M., 2008. Sediment supply and fluxes in glacial and outwash fjords, Kongsfjorden and Adventfjorden, Svalbard. *Polish Polar Research* 29 (1), 59–72.

## Chapter 4

### Summary and conclusions

#### 4.1 Conclusions

The simulated circulation pattern showed a buoyant jet issuing from the tunnel, a vertically buoyant plume and a horizontal surface plume forming part of an estuarine circulation. This structure was observed for a combination of submergence ratios and Froude numbers that determined the buoyant jets to be stable.

The quantities that describe the estuarine circulation are quantitatively related to the characteristics of the subglacial buoyant jet, represented by the Froude number. The range of  $Fr$  numbers set in these experiments is similar to what Syvitski (1989) described as "Fr ~ 0" conditions. A further improvement of the description provided by this rather qualitative model is achieved when considering the relative submergence  $H/d$ , given that this ratio, along with  $Fr$  and the jet angle  $\theta$ , determines the structure and dilution of buoyant jets in confined depth (Jirka and Harleman, 1973).

Buoyancy is the main forcing that, within the range of  $Fr$  set in this study, drives the estuarine circulation in glacial fjords, even for the case of momentum-dominated jets. This result would be produced by the rapid loss of momentum after the jet issues into the ambient

water, as stated by some authors (Fischer et al., 1979; List, 1982). In the context of global warming, this implies that the circulation in glacial fjords could intensify as result of higher freshwater discharges caused by increased ice melting rates.

Momentum-dominated experiments demonstrated to be more sensitive to the presence suspended sediment in the discharge than buoyancy-dominated experiments. This situation is caused by a lowered buoyancy caused by the presence of sediment in the buoyant discharge and the little difference from the ambient water density. It is likely that such a condition could be observed in nature when the discharges are sediment-laden and have a rapid flow (Russell and Arnott, 2003). As buoyancy becomes the dominant forcing, more sediment is necessary to produce any significant effect in the estuarine circulation and the characteristics of the plumes.

At high concentrations the sediment settled in the far field in the form of "fingering" or convective sedimentation. This process was highly effective removing sediment from the surface layer and showed deposition rates that are noticeably higher than produced by flocculation alone.

Despite fine sediment settled in the far field, the "clouds" of sediment were transported back to the near field by the landward estuarine current. This result differs with the statement that fine sediment settles in the far field and sets out questions for further studies.

Flocculation is an important process that is necessary to include when dealing with fine sediment transport. The effect of not including flocculation is a completely different pattern of distribution and the absence of important processes such as sediment induced instabilities.

The results obtained with thesis showed the existence of a relationship between the characteristics of the buoyant jet and those of the associated estuarine circulation. Other forcings and conditions, however, will modulate this interaction. Thus future experiments should include subglacial buoyant discharges in a stratified fjord and the effect of tides

in order to approach more realistic situations. Also, simulations of pulse-like discharges would allow better representation of the discontinuous nature of these discharges.

A two dimensional nonhydrostatic proved to be a very useful tool to study the structure of subglacial discharges and the estuarine circulation in glacial fjords, given the characteristic scales and dimensions of these systems. In nature, however, there is a third dimension that was not considered in these experiments but can provide more information about the evolution of these discharges in future studies. Vortices and eddies were observed in the near field during the initial stages of the experiments. Once the experiments reached the steady state, vortices and eddies disappeared but some KH instabilities remained in the near field. In spite of being a 2D model and the inherent limitation to represent processes that are essentially 3D, like vortex stretching, the model and grid resolution allowed to reproduce features like KH instabilities, vortices and vortex dipoles.

In spite of the oversimplification and fundamental focus of this investigation, the obtained results can provide a way to estimate the consequences of modifying the buoyant jet characteristics and relative submergence on the associated estuarine circulation and fine sediment transport.

## 4.2 Future work

The numerical experiments carried out during this work did not consider salinity nor temperature in the interaction between the buoyant jet and the ambient water but only included directly density as the tracer. Considering the importance that some author have attributed to the temperature difference in the ice melting and production of buoyant plumes at the face of tidewater glaciers, future studies should include the temperature, salinity and the state equation in order to depict the circulation in glacial fjords under the effect of varying ambient temperature.

The possibility of including different sediment fractions in the model would allow for simulations of discharges including a range of sediment size from coarser to finer sediment. In this sense, it would be possible to represent processes from the interaction between different fractions, such as differential settling.

An important result of this thesis was the simulation of convective sedimentation. A next step should also involve salinity and temperature variations to get the instabilities, in order to represent more realistic conditions and compare with experimental observations from literature.

As flocculation is a necessary process to be included when modeling fine-sediment transport, a following step should explore other expressions for flocculation, specially, the recent equations that combine the effect of turbulence and sediment concentration on the settling velocity.

## Chapter 5

### Bibliography

Angirasa, D., 1999. Interaction of low-velocity plane jets with buoyant convection adjacent to heated vertical surfaces. *Numerical Heat Transfer, Part A* 35, 67–84.

Anwar, H. O., 1973. Two-dimensional buoyant jet in a current. *Journal of Engineering Mathematics* 7 (4), 297 – 311.

Apollonio, S., 1973. Glaciers and nutrients in arctic seas. *Science* 180 (4085), 491 – 493.

Arakeri, J., Das, D., Srinivasan, J., 2000. Bifurcation in a buoyant horizontal laminar jet. *Journal of Fluid Mechanics* 412, 61–73.

Ashley, G. M., Smith, N. D., 2000. Marine sedimentation at a calving glacier margin. *Geological Society of America Bulletin* 112 (5), 657–667.

Awad, E., Toorman, E., Lacor, C., 2008. Large eddy simulations for quasi-2d turbulence in shallow flows: A comparison between different subgrid scale models. *Journal of Marine Systems* 77, 511–528.

Batchelor, G. K., 1969. Computation of the energy spectrum in homogeneous two-dimensional turbulence. *Physics of Fluids* 12, 2–233.

- Bourgault, D., Kelley, D. E., 2004. A laterally averaged nonhydrostatic ocean model. *Journal of Atmospheric and Oceanic Technology* 21, 1910–1924.
- Bursik, M. I., 1995. Theory of the sedimentation of suspended particles from fluvial plumes. *Sedimentology* 42, 831–838.
- Burt, T. N., 1986. Field settling velocities of mud. In: Mehta, A. J. (Ed.), *Estuarine cohesive sediment dynamics. Lecture notes on coastal and estuarine studies*. Springer-Verlag, pp. 126–150.
- Carey, S. N., Sigurdsson, H., Sparks, R. S. J., 1988. Experimental studies of particle-laden plumes. *Journal of Geophysical Research* 93 (B12), 15,314–15,328.
- Carney, D., Oliver, J. S., Armstrong, C., 1999. Sedimentation and composition of wall communities in Alaskan fjords. *Polar Biology* 22, 38 – 49.
- Chen, C. J., Rodi, W., 1980. *Vertical turbulent buoyant jets – A review of experimental data*. Pergamon Press.
- Comiso, J., 2002. A rapidly declining perennial sea ice cover in the Arctic. *Geophysical Research Letters* 29 (20), 13,219–13,234, doi:10.1029/2002GL015650.
- Cowan, E. A., 1992. Meltwater and tidal currents: Controls on circulation in a small glacial fjord. *Estuarine, Coastal and Shelf Science* 34, 381–392.
- Cowan, E. A., Powell, R. D., 1990. Suspended sediment transport and deposition of cyclically interlaminated sediment in a temperate glacial fjord, Alaska, U.S.A. Geological Society, London, Special Publications 53, 75–89.
- Cowan, E. A., Powell, R. D., 1991. Ice-proximal sediment accumulation rates in a temperate glacial fjord, southeastern Alaska. In: Anderson, J. B., Ashley, G. M. (Eds.), *Glacial*

marine sedimentation; Paleoclimatic significance. Vol. 251. Geological Society of America Special Paper, pp. 61–73.

Cowan, E. A., Powell, R. D., Smith, N. D., 1988. Rainstorm-induced event sedimentation at the tidewater front of a temperate glacier. *Geology* 16, 409–412.

Curran, K., Hill, P., Milligan, T., Cowan, E., Syvitski, J., Konings, S., 2004. Fine-grained sediment flocculation below the Hubbard Glacier meltwater plume, Disenchantment Bay, Alaska. *Marine Geology* 203, 83–94.

Cushman-Roisin, B., 1994. Introduction to geophysical fluid dynamics. Prentice Hall.

Cuthbertson, A. J. S., Davies, P. A., 2008. Deposition from particle-laden, round, turbulent, horizontal, buoyant jets in stationary and coflowing receiving fluids. *Journal of Hydraulic Engineering* 134 (4), 390–402.

Cuthbertson, Alan J. S. and Apsley, D. D., Davies, P. A., Lipari, G., Stansby, P. K., 2008. Deposition from particle-laden, plane, turbulent, buoyant jets. *Journal of Hydraulic Engineering* 134 (8), 1110–1122.

Domack, E. W., Foss, D. J. P., Syvitski, J. P. M., McClennen, C. E., 1994. Transport of suspended particulate matter in an Antarctic fjord. *Marine Geology* 121, 161–170.

Domack, E. W., Williams, C. R., 1990. Fine structure and suspended sediment transport in three Antarctic fjords. *Antarctic Research Series* 50, 71–89.

Dowdeswell, J. A., 1986. The distribution and character of sediments in a tidewater glacier, Southern Baffin Island, N.W.T., Canada. *Arctic and Alpine Research* 18 (1), 45–56.

Dyer, K. R., 1988. Fine sediment particle transport. In: Job, D., van Leussen, W. (Eds.), *Physical Processes in Estuaries*. Springer-Verlag, pp. 295–310.

- Dyer, K. R., 1995. Sediment transport processes in estuaries. In: Perillo, G. M. E. (Ed.), *Geomorphology and Sedimentology of Estuaries. Developments in Sedimentology*, 53. Elsevier, pp. 423–449.
- Dyer, K. R., Bale, A. J., Christie, M. C., Feates, N., Jones, S., Manning, A. J., 2002. The turbidity maximum in a mesotidal estuary, the Tamar estuary, UK: II. the flocc properties. In: Winterwerp, J. C., Kranenburg, C. (Eds.), *Fine sediment dynamics in the marine environment*. Elsevier, pp. 219–232.
- Elverhøi, A., Lønne, Ø., Seland, R., 1983. Glaciomarine sedimentation in a modern fjord environment, Spitsbergen. *Polar Research* 1 (2), 127–149.
- Ernst, G. G. J., Sparks, R. S. J., Carey, S. N., Bursik, M. I., 1996. Sedimentation from turbulent jets and plumes. *Journal of Geophysical Research* 101 (B3), 5575–5589.
- Etherington, L. L., Hooge, P. N., Hooge, E. R., Hill, D. F., 2007. Oceanography of Glacier Bay, Alaska: Implications for biological patterns in a glacial fjord estuary. *Estuaries and Coasts* 30 (6), 927–944.
- Farmer, D. M., Freeland, H. J., 1983. The physical oceanography of fjords. *Progress in Oceanography* 12, 147–220.
- Fetzer, I., Lønne, O. J., Pearson, T., 2002. The distribution of juvenile benthic invertebrates in an Arctic glacial fjord. *Polar Biology* 25, 303–315.
- Fischer, H., List, E. J., Koh, R. C. Y., Imberger, J., Brooks, N. H., 1979. *Mixing in inland and coastal waters*. Academic Press.
- Gallacher, P. C., Piacsek, S., Dietrich, D., 2001. Hydrostatic and nonhydrostatic simulations of buoyantly driven coastal jets. In: Spaulding, M. L. (Ed.), *Proceedings of the*

Seventh International Conference, November 5-7, 2001, St. Petersburg, Florida. pp. 204-214.

Gilbert, R., 1978. Observations on oceanography and sedimentation at Pangnirtung fjord, Baffin Island. *Maritime Sediments* 14 (1), 1-9.

Gilbert, R., 1982. Contemporary sedimentary environments on Baffin Island, N.W.T., Canada: Glaciomarine processes in fiords of Eastern Cumberland Peninsula. *Arctic and Alpine Research* 14 (1), 1-12.

Gilbert, R., 1983. Sedimentary processes of Canadian Arctic fjords. *Sedimentary Geology* 36, 147-175.

Gilbert, R., Nielsen, N., Möller, H., Desloges, J. R., Rasch, M., 2002. Glaciomarine sedimentation in Kangerdluk (Disko Fjord), West Greenland, in response to a surging glacier. *Marine Geology* 191, 1-18.

Görllich, K., Węślawski, J. M., Zajączkowski, M. J., 1987. Suspension settling effect on macrobenthos biomass distribution in the Hornsund fjord, Spitsbergen. *Polar Research* 5, 175-192.

Green, T., 1987. The importance of double diffusion to the settling of suspended material. *Sedimentology* 34 (2), 319-331.

Greisman, P., 1979. On upwelling driven by the melt of ice shelves and tidewater glaciers. *Deep-Sea Research* 26A, 1051-1065.

Grella, J. J., Faeth, G. M., 1975. Measurements in a two-dimensional thermal plume along a vertical adiabatic wall. *Journal of Fluid Mechanics* 71, 701-710.

Haidvogel, D. B., Beckmann, A., 1999. *Numerical Ocean Circulation Modeling*. Imperial College Press.

- Hallet, B., Hunter, L., Bogen, J., 1996. Rates of erosion and sediment evacuation by glaciers: A review of field data and their implications. *Global and Planetary Change* 12, 213–235.
- Hartley, C. H., Dunbar, M. J., 1938. On the hydrographic mechanism of the so-called brown zones associated with tidal glaciers. *Journal of Marine Research* 1, 305–311.
- He, S., Xu, Z., Jackson, J., 2002. An experimental investigation of buoyancy-opposed wall jet flow. *International Journal of Heat and Fluid Flow* 23, 487–496.
- Hein, F. J., Syvitski, J. P. M., 1992. Sedimentary environments and facies in an arctic basin, Itirbilung Fiord, Baffin Island, Canada. *Sedimentary Geology* 81, 17–45.
- Hill, D., Ciavola, S., Etherington, L., Klaat, M., 2009. Estimation of freshwater runoff into Glacier Bay, Alaska and incorporation into a tidal circulation model. *Estuarine, Coastal and Shelf Science* 82, 95–107.
- Hill, P. S., Milligan, T. G., Geyer, W. R., 2000. Controls on effective settling velocity of suspended sediment in the Eel River flood plume. *Continental Shelf Research* 20, 2095–2111.
- Hill, P. S., Syvitski, J. P., Cowan, E. A., Powell, R. D., 1998. In situ observations of floe settling velocities in Glacier Bay, Alaska. *Marine Geology* 145, 85–94.
- Holland, D. M., Thomas, R. H., deYoung, B., Ribergaard, M. H., Lyberth, B., 2008. Acceleration of Jakobshavn Isbræ triggered by warm subsurface ocean waters. *Nature Geoscience* 1, 659–664.
- Hooge, P. N., Hooge, E. R., 2002. Fjord oceanographic processes in glacier bay, alaska. USGS - Alaska Science Center, 144 pp.

Hop, H., Pearson, T., Hegseth, E. N., Kovacs, K. M., Wiencke, C., Kwasniewski, S., Eliane, K., Mehlum, F., Gulliksen, B., Wlodarska-Kowalczuk, M., Lydersen, C., Weslawski, J. M., Cochrane, S., Gabrielsen, G. W., Leakey, R. J. G., Lønne, O. J., Zajaczkowski, M., Falk-Petersen, S., Kendall, M., Wängberg, S.-Å., Bischof, K., Voronkov, A. Y., Kovaltchouk, N. A., Wiktor, J., Poltermann, M., Di Prisco, G., Papucci, C., Gerland, S., 2002. The marine ecosystem of Kongsfjorden, Svalbard. *Polar Research* 21 (1), 167–208.

Horne, E. P. W., 1985. Ice-induced vertical circulation in an Arctic fjord. *Journal of Geophysical Research* 90, 1078–1086.

Hoskin, C. M., Burrell, D. C., Freitag, G. R., 1978. Suspended sediment dynamics in Blue Fjord, Western Prince William Sound, Alaska. *Estuarine and Coastal Marine Science* 7, 1–16.

Hoyal, D. C. J. D., Bursik, M. I., Atkinson, J. F., 1999. The influence of diffusive convection on sedimentation from buoyant plumes. *Marine Geology* 159, 205–220.

Huai, W., Li, Z., Qian, Z., Zeng, Y., Han, J., 2010. Numerical simulation of horizontal buoyant wall jet. *Journal of Hydrodynamics* 22, 58–65.

Huang, M.-J., 2001. Enstrophy cascade and Smagorinsky model of 2d turbulent flows. *The Chinese Journal of Mechanics* 17 (3), 121–129.

Jaeger, J. M., Nittrouer, C. A., 1999. Sediment deposition in an Alaskan fjord: Controls on the formation and preservation of sedimentary structures in Icy Bay. *Journal of Sedimentary Research* 69 (5), 1011–1026.

Jirka, G. H., 1982. Turbulent buoyant jets in shallow fluid layers. In: Rodi, W. (Ed.), *Turbulent buoyant jets and plumes*. Pergamon Press, pp. 69–120.

Jirka, G. H., Harleman, D. R. F., 1973. The mechanics of submerged multiport diffusers for buoyant discharges in shallow waters. Tech. Rep. Technical Report 169, Ralph M. Parsons Laboratory for Water Resources and Hydrodynamics, Massachusetts Institute of Technology, Cambridge, Massachusetts.

Jirka, G. H., Harleman, D. R. F., 1979. Stability and mixing of a vertical plane buoyant jet in confined depth. *Journal of Fluid Mechanics* 94, 275–304.

Josberger, E. G., 1978. A laboratory and field study of iceberg deterioration. In: Hussein, A. A. (Ed.), *Iceberg utilization. Proceedings of the first international conference*, Ames, Iowa, 1977. Pergamon Press, pp. 245–264.

Josberger, E. G., Martin, S., 1981. A laboratory and theoretical study of the boundary layer adjacent to a vertical melting ice wall in salt water. *Journal of Fluid Mechanics* 111, 439–473.

Josberger, E. G., Neshyba, S., 1980. Iceberg melt-driven convection inferred from field measurements of temperature. *Annals of glaciology* 1, 113–117.

Komar, P., 1976. Suspended sediment transport and mud deposition on continental shelf. In: Stanley, D. J., P., S. D. J. (Eds.), *Marine sediment transport and environmental management*. John Wiley and Sons, pp. 127–158.

Koppes, M. N., Hallet, B., 2002. Influence of rapid glacial retreat on the rate of erosion by tidewater glaciers. *Geology* 30 (1), 47–50.

Krumbein, W. C., Sloss, L. L., 1963. *Stratigraphy and sedimentation*, 2nd Edition. W. H. Freeman.

Kuang, C. P., Lee, J. H. W., 2001. Effect of downstream control on stability and mixing of a vertical plane buoyant jet in confined depth. *Journal of Hydraulic Research* 39, 375–391.

- Kuang, C. P., Lee, J. H. W., 2006. Stability and mixing of a vertical axisymmetric buoyant jet in shallow water. *Environmental Fluid Mechanics* 6, 153–180.
- Kuijper, C., Cornelisse, J. M., Winterwerp, J. C., 1989. Research on erosive properties of cohesive sediments. *Journal of Geophysical Research* 94, 14,341–14,350.
- Kundu, P. K., 1990. *Fluid Mechanics*. Academic Press.
- Lai, M. C., Faeth, G. M., 1987. Turbulence structure of vertical adiabatic wall plumes. *Journal of Heat Transfer* 109, 663–670.
- Lai, M. C., Jeng, S. M., Faeth, G. M., 1986. Structure of turbulent adiabatic wall plumes. *Journal of Heat Transfer* 108, 827–834.
- Lane-Serff, G. F., 2011. Deposition of cohesive sediment from turbulent plumes, gravity currents and turbidity currents. *Journal of Hydraulic Engineering (In Press)*, doi:10.1061/(ASCE)HY.1943-7900.0000463.
- Lane-Serff, G. F., Moran, T. J., 2005. Sedimentation from buoyant jets. *Journal of Hydraulic Engineering* 131 (3), 166–174, doi:10.1061/(ASCE)0733-9429(2005)131:3(166).
- Lee, J. H. W., Jirka, G. H., 1981. Vertical round buoyant jet in shallow depth. *Journal of the Hydraulics Division, ASCE* 107, 1651–1675.
- Lee, W. T., Lee, J. H. W., 1998. Effect of lateral confinement on initial dilution of vertical round buoyant jet. *Journal of Hydraulic Engineering* 124, 263–279.
- List, E. J., 1982. Turbulent jets and plumes. *Annual Review in Fluid Mechanics* 14, 189–212.
- Liu, W.-C., 2005. Modeling the influence of settling velocity on cohesive sediment transport in Tanshui River estuary. *Environmental Geology* 47, 535–546, doi:10.1007/s00254-004-1176-z.

- Ljuboja, M., Rodi, W., 1981. Prediction of horizontal and vertical turbulent buoyant wall jets. *Journal of Heat Transfer* 103, 343–349.
- MacAyeal, D. R., 1985. Evolution of tidally triggered meltwater plumes below ice shelves. *Antarctic Research Series* 43, 109–132.
- Mackiewicz, N. E., Powell, R. D., Carlson, P. R., Molnia, B. F., 1984. Interlaminated ice-proximal glacial marine sediments in Muir Inlet, Alaska. *Marine Geology* 57, 113–147.
- Manning, A. J., Friend, P. L., Prowse, N., Amos, C. L., 2007. Estuarine mud flocculation properties determined using an annular mini-flume and the LabSFLOC system. *Continental Shelf Research* 27, 1080–1095.
- Markofsky, M., Westrich, B., 2007. Transport modeling. In: Westrich, B., Ulrich, F. (Eds.), *Sediment Dynamics and Pollutant Mobility in Rivers. An Interdisciplinary Approach*. Springer, pp. 117–169.
- Marshall, J., Hill, C., Perelman, L., Adcroft, A., 1997. Hydrostatic, quasi-hydrostatic, and nonhydrostatic ocean modeling. *Journal of Geophysical Research* 102 (C3), 5733–5752.
- Matthews, J., Quinlan, A., 1975. Seasonal characteristics of water masses in Muir Inlet, a fjord with tidewater glaciers. *Journal of the Fisheries Research Board of Canada* 32, 1693–1703.
- McAnally, W. H., Mehta, A. J., 2001. Seasonal variability of sediment erodibility and properties on a macrotidal mudflat, Peterstone Wentloogw, Severn estuary, UK. In: Mitchener, H. J., O'Brien, D. J. (Eds.), *Coastal and estuarine fine sediment processes*. Elsevier, pp. 301–322.
- McCool, W. W., Parsons, J. D., 2004. Sedimentation from buoyant fine-grained suspensions. *Continental Shelf Research* 24, 1129–1142, doi:10.1016/j.csr.2004.03.009.

- Mehta, A. J., 1986. Characterization of cohesive sediment properties and transport processes in estuaries. In: Mehta, A. J. (Ed.), *Estuarine cohesive sediment dynamics*. Lecture notes on coastal and estuarine studies. Springer-Verlag, pp. 290–325.
- Mehta, A. J., 1989. On estuarine cohesive sediment suspension behavior. *Journal of Geophysical Research* 94 (C10), 14,303–14,3014.
- Mortensen, J., Lennert, K., Bendtsen, J., Rysgaard, S., 2011. Heat sources for glacial melt in a sub-Arctic fjord (Godthåbsfjord) in contact with the Greenland Ice Sheet. *Journal of Geophysical Research* 116 (C01013), doi:10.1029/2010JC006528.
- Morton, B. R., 1959. Forced plumes. *Journal of Fluid Mechanics* 5, 151–163.
- Motyka, R. J., Hunter, L., Echelmeyer, K. A., Connor, C., 2003. Submarine melting at the terminus of a temperate tidewater glacier, LeConte Glacier, Alaska, U.S.A. *Annals of Glaciology* 36, 57–65.
- Mugford, R. I., Dowdeswell, J., 2007. Numerical modelling of glacial marine sedimentation from tidewater glaciers: iceberg-rafted vs meltwater plume deposition. *Geophysical Research Abstracts* 9 (10297).
- Mugford, R. I., Dowdeswell, J. A., 2011. Modeling glacial meltwater plume dynamics and sedimentation in high-latitude fjords. *Journal of Geophysical Research* 116 (F01023), doi:10.1029/2010JF001735.
- Neshyba, S., 1977. Upwelling by icebergs. *Nature* 267 (5611), 507–508.
- Neshyba, S., Josberger, E. G., 1980. On the estimation of Antarctic iceberg melt rate. *Journal of Physical Oceanography* 10, 1681–1685.
- O'Donnell, J., 2010. The dynamics of estuary plumes and fronts. In: Valle-Levinson, A. (Ed.), *Contemporary issues in estuarine physics*. Cambridge, pp. 186–246.

- Oerlemans, J., 1993. Quantifying global warming from the retreat of glaciers. *Science* 264, 243–245.
- Ozgekmen, T. M., Iliescu, T., Fischer, P. F., Srinivasan, A., Duan, J., 2007. Large eddy simulation of stratified mixing in two-dimensional dam-break problem in a rectangular enclosed domain. *Ocean Modelling* 16, 106140.
- Parsons, J. D., Bush, J. W. M., Syvitsky, J. P. M., 2001. Hyperpycnal plume formation from riverine outflows with small sediment concentrations. *Sedimentology* 48, 465–478.
- Parsons, J. D., Garcia, M. H., 2001. Enhanced sediment scavenging due to double-diffusive convection. *Journal of Sedimentary Research* 70 (1), 47–52.
- Partheniades, E., 1965. Erosion and deposition of cohesive soils. *Journal of the Hydraulics Division* 91, 105–139.
- Partheniades, E., 1986. Fundamental framework for cohesive sediment dynamics. In: Mehta, A. J. (Ed.), *Estuarine cohesive sediment dynamics. Lecture notes on coastal and estuarine studies*. Springer-Verlag, pp. 219–250.
- Peizhen, Z., Molnar, P., Downs, W. R., 2001. Increased sedimentation rates and grain sizes 2 – 3 Myr ago due to the influence of climate change on erosion rates. *Nature* 410, 891–897.
- Pejrup, M., Mikkelsen, O. A., 2010. Factors controlling the field settling velocity of cohesive sediment in estuaries. *Estuarine, Coastal and Shelf Science* 87, 177–185.
- Pfirman, S. L., Solheim, A., 1989. Subglacial meltwater discharge in the open-marine tidewater glacier environment: Observations from Nordaustlandet, Svalbard Archipelago. *Marine Geology* 86, 265–281.

- Pichlmaier, M., Aquino, F. E., Da-Silva, C. S., Braun, M., 2004. Suspended sediments in Admiralty Bay, King George Island (Antarctica). *Pesquisa Antartica Brasileira* 4, 77–85.
- Pickard, G. L., 1967. Some oceanographic characteristics of the larger inlets of southeast Alaska. *Journal of the Fisheries Research Board, Canada* 24, 1475–1505.
- Powell, R. D., 1990. Glacimarine processes at grounding-line fans and their growth to ice-contact deltas. In: Dowdeswell, J. A., Scourse, J. D. (Eds.), *Glacimarine Environments: Processes and Sediments*. Geological Society Special Publication. Vol. 53. The Geological Society, pp. 53–73.
- Puls, W., Kuehl, H., Heymann, K., 1988. Settling velocity of mud flocs: results of field measurements in the Elbe and the Wesser estuary. In: Dronkers, J., van Leussen, W. (Eds.), *Physical Processes in Estuaries*. Springer-Verlag, pp. 404–424.
- Reed, D. J., 1988. Tidal currents and glacial discharge, laguna san rafael, southern chile. *Journal of Coastal Research* 4 (1), 93–102.
- Richardson, J. F., Zaki, W. N., 1954. The sedimentation of a suspension of uniform spheres under conditions of viscous flow. *Chemical Engineering Science* 3 (2), 65–73.
- Rignot, E., Koppes, M., Velicogna, I., 2010. Rapid submarine melting of the calving faces of West Greenland glaciers. *Nature Geoscience* 3, 187–191, doi:10.1038/NGEO765.
- Russell, H., Arnott, R., 2003. Hydraulic-jump and hyperconcentrated-flow deposits of a glaciogenic subaqueous fan: Oak Ridges Moraine, southern Ontario, Canada. *Journal of Sedimentary Research* 73 (6), 887–905.
- Salcedo-Castro, J., Bourgault, D., Bentley, S., deYoung, B., 2011a. Modeling ice-proximal fine sediment transport associated with a subglacial buoyant jet in glacial fjords: A fundamental approach. *Marine Geology* (*Submitted*).

Salcedo-Castro, J., Bourgault, D., deYoung, B., 2011b. Circulation induced by subglacial discharge in glacial fjords: Results from idealized numerical simulations. *Continental Shelf Research* 31, 1396–1406.

Sangras, R., Dai, Z., Faeth, G. M., 1998. Mixing structure of plane self-preserving buoyant turbulent plumes. *Journal of Heat Transfer* 120, 1033–1041.

Sangras, R., Dai, Z., Faeth, G. M., 1999. Mixture fraction statistics of plane self-preserving buoyant turbulent adiabatic wall plumes. *Journal of Heat Transfer* 121, 837–843.

Sangras, R., Dai, Z., Faeth, G. M., 2000. Velocity statistics of plane self-preserving buoyant turbulent adiabatic wall plumes. *Journal of Heat Transfer* 122, 693–700.

Sexton, D. J., Dowdeswell, J. A., Solheim, A., Elverhøi, A., 1992. Seismic architecture and sedimentation in northwest Spitsbergen fjords. *Marine Geology* 103, 53–68.

Sharp, J. J., Vyas, B. D., 1977. The buoyant wall jet. *Proceedings of the Institution of Civil Engineers, Part 2* 63, 593–611.

Shaw, P.-T., Chao, S.-Y., 2006. A nonhydrostatic primitive-equation model for studying small-scale processes: An object-oriented approach. *Continental Shelf Research* 26, 1416–1432.

Shi, Z., Zhou, H. J., 2004. Controls on effective settling velocities of mud flocs in the Changjiang Estuary, China. *Hydrological Processes* 18, 2877–2892.

Simpson, J. H., Allen, C. M., Morris, N. C. G., 1978. Fronts on the continental shelf. *Journal of Geophysical Research* 83, 4607–4614.

Smagorinsky, J., 1963. General circulation experiments with primitive equations. I. The basic experiment. *Monthly Weather Review* 91, 99–164.

- Sobey, R. J., J., J. A., Keane, R. D., 1988. Horizontal round buoyant jet in shallow water. *Journal of Hydraulic Engineering* 114 (8), 910–929.
- Solomon, S., Qin, D., Manning, M., Chen, Z., Marquis, M., Averyt, K. B., Tignor, M., Miller, H. L. (Eds.), 2007. *Contribution of Working Group I to the Fourth Assessment Report of the Intergovernmental Panel on Climate Change, 2007*. Cambridge University Press.
- Sorteberg, A., Kvingedal, B., 2006. Atmospheric forcing on the Barents Sea winter ice extent. *Journal of Climate* 19, 4772–4784.
- Sparks, R. S. J., Carey, S. N., Sigurdsson, H., 1991. Sedimentation from gravity currents generated by turbulent plumes. *Sedimentology* 38, 839–856.
- Straneo, F., Curry, R. G., Sutherland, D. A., Hamilton, G. S., Cenedese, C., Våge, K., Stearns, L. A., 2011. Impact of fjord dynamics and glacial runoff on the circulation near Helheim Glacier. *Nature Geoscience* 4, 322–327, doi:10.1038/NGEO1109.
- Straneo, F., Hamilton, G. S., Sutherland, D. A., Stearns, L. A., Davidson, F., Hammill, M. O., Stenson, G. B., Rosing-Asvid, A., 2010. Rapid circulation of warm subtropical waters in a major glacial fjord in East Greenland. *Nature Geoscience* 3, 182–186, doi:10.1038/NGEO764.
- Svendsen, H., Beszczynska-Møller, A., Hagen, J. O., Lefauconnier, B., Tverberg, V., Gerland, S., Børre-Orbæk, J., Bischof, K., Papucci, C., Zajaczkowski, M., Azzolini, R., Bruland, O., Wiencke, C., Winther, J. G., Dallmann, W., 2002. The physical environment of Kongsfjorden-Krossfjorden, an Arctic fjord system in Svalbard. *Polar Research* 21, 133–166.
- Syvitski, J., Burrell, D. C., Skei, J. M., 1987. *Fjords: processes and products*. Springer-Verlag.

Syvitski, J. P. M., 1989. On the deposition of sediment within glacier-influenced fjords: Oceanographic controls. *Marine Geology* 85, 301–329.

Syvitski, J. P. M., Andrews, J. T., 1994. Climate change: Numerical modelling of sedimentation and coastal processes, eastern Canadian Arctic. *Arctic and Alpine Research* 26 (3), 199–212.

Syvitski, J. P. M., Murray, J. W., 1981. Particle interaction in fjord suspended sediment. *Marine Geology* 39, 215–242.

Szczuciński, W., Zajączkowski, M., Scholten, J., 2009. Sediment accumulation rates in subpolar fjords-Impact of post-Little Ice Age glaciers retreat, Billefjorden, Svalbard. *Estuarine, Coastal and Shelf Science* 85, 345–356.

Thorpe, S. A., 1968. A method of producing a shear flow in a stratified fluid. *Journal of Fluid Mechanics* 32, 693–704.

Trusel, L. D., Powell, R. D., Cumpston, R. M., Brigham-Grette, J., 2010. Modern glacialine processes and potential future behaviour of Kronebreen and Kongsvegen polythermal tidewater glaciers, Kongsfjorden, Svalbard. In: Howe, J. A., Austin, W. E. N., Forwick, M., Paetzel, M. (Eds.), *Fjord Systems and Archives*. Vol. 344. Geological Society, London, Special Publications, pp. 89–102.

van der Veen, C. J., 2002. Observations of wind influence on exchange flows in a strait of the Chilean Inland Sea. *Progress in Physical Geography* 26 (1), 96–122.

Van Leussen, W., 1994. Estuarine macro flocs and their role in the Dollard estuary, The Netherlands. Ph.D. thesis, Utrecht University, The Netherlands.

van Rijn, L. C., 2007. Unified view of sediment transport by currents and waves. I: Initiation of motion, bed roughness, and bed-load transport. *Journal of Hydraulic Engineering* 133 (6), 649–667.

Verney, R., Lafite, R., Brun-Cottan, J.-C., 2009. Flocculation potential of estuarine particles: The importance of environmental factors and of the spatial and seasonal variability of suspended particulate matter. *Estuaries and Coasts* 32, 678–693.

Vieli, A., 2011. Calvin glaciers. In: Singh, V. P., Singh, P., Haritashya, U. K. (Eds.), *Encyclopedia of Snow, Ice and Glaciers*. Springer, pp. 1175–1179.

Walters, R. A., Josberger, E. G., Driedger, C. L., 1988. Columbia Bay, Alaska: An 'upside down' estuary. *Estuarine, Coastal and Shelf Science* 26, 607–617.

Wang, X. H., Byun, D. S., Wang, X. L., Chod, Y. K., 2005. Modelling tidal currents in a sediment stratified idealized estuary. *Continental Shelf Research* 25, 655–665.

Warren, C. R., 2011. Calvin glaciers. In: Singh, V. P., Singh, P., Haritashya, U. K. (Eds.), *Encyclopedia of Snow, Ice and Glaciers*. Springer, pp. 105–106.

Wentworth, C. K., 1922. A scale of grade and class terms for clastic sediments. *The Journal of Geology* 30 (5), 377–392.

Winterwerp, J. C., 2002. On the flocculation and settling velocity of estuarine mud. *Continental Shelf Research* 22, 1339–1360.

Węslawski, J. M., Legeżyńska, J., 1998. Glaciers caused zooplankton mortality? *Journal of Plankton Research* 20 (7), 1233–1240.

Wright, S. J., Roberts, P. J. W., Zhongmin, Y., Bradley, N. E., 1991. Surface dilution of round submerged buoyant jets. *Journal of Hydraulic Research* 29, 67–89.

You, Z.-J., 2004. The effect of suspended sediment concentration on the settling velocity of cohesive sediment in quiescent water. *Ocean Engineering* 31, 1955-1965.

Zaborska, A., Pempkowiak, J., Papucci, C., 2006. Some sediment characteristics and sedimentation rates in an Arctic fjord (Kongsfjorden, Svalbard). *Środkowo-Pomorskie Towarzystwo Naukowe Ochrony Środowiska* 8 (80-97).

Zajączkowski, M., 2008. Sediment supply and fluxes in glacial and outwash fjords, Kongsfjorden and Adventfjorden, Svalbard. *Polish Polar Research* 29 (1), 59-72.

Zajączkowski, M. J., Legeżyńska, J., 2001. Estimation of zooplankton mortality caused by an Arctic glacier outflow. *Oceanologia* 43 (3), 341-351.



